Experimental Analysis of Power Control and Element Spacing for Unobtrusive MIMO Antenna Systems

A Thesis

Submitted to the Faculty

of

Drexel University

by

Nicholas J. Kirsch

in partial fulfillment of the

requirements for the degree

of

Doctor of Philosophy

June 2009

Dedications

To my parents,
Richard and Linda,
and to my sister, Emily.

Acknowledgements

When I stand at the summit of a mountain and look back upon the path I traveled, I am always amazed by the clarity of the path. Looking back to the trailhead over the route, the obstacles and challenges are easy to point out. However, there are many struggles during the climb and the trail is not always clear. While one climbs under his own power, the summit can only be gained with the help of those who have the experience and foresight to be successful. It is gained with the help from those who support you when the journey is most dire.

Many people have given me hand on my path through graduate school. I owe all of those who have climbed with me my deepest gratitude.

Over the past six years, I have received exceptional support at Drexel University. The College of Engineering has been a very hospitable place and I would like to thank Dr. Mun Choi, whose conversations helped me understand the bigger picture of academia. Many thanks also go to Dr. Robert Koerner and all of the Koerner family for providing me with funding and career guidance.

I have been tremendously fortunate to be surrounded by many stellar academics and friends (often one and the same) at Drexel University. The Department of Electrical and Computer Engineering is full of talented faculty, most of whom have aided me in some way. I would like to thank Dr. Moshe Kam whose intelligence, wisdom, and vision are inspiring. My education is all the better for having had the opportunity to work and learn from him. Many thanks to Dr. Jaudelice C. de Oliveira who is a teacher and for giving me the opportunity to instruct a course. I am also thankful for learning and working with Dr. William Regli.

Dr. Timothy Kurzweg made my first steps in graduate school possible. His call opened the doors to Drexel University for me. It has been a pleasure to work with

him on several research projects and to go to some great concerts. I also would like to thank Dr. Steven Weber. He is an outstanding teacher, academic, and (perhaps most importantly) fellow Wisconsin native.

I avoided many missteps in completing my degree with the help of the terrific ECE staff of Ms. Tanita Chapelle, Ms. Stacey Caiazzo, Ms. Dolores Watson, Mr. Chad Morris, and Ms. Kathy Bryant.

I would like to thank my classmates, my labmates, and my friends that have been on this climb alongside me while they were immersed in their own studies. They come from the corners of the earth and have shared more with me than just solving research problems. My graduate studies were much easier and enjoyable with your companionship. I extend my thanks to Mr. Sumant Kawale, Dr. Chao Liang, Dr. Daniele Piazza, Mr. Abhishek Khemka, Mr. John Kountouriotis, Mr. Doug Pfiel, Mr. Prathaban Mookiah, Mr. Kevin Wanuga, Mr. Boris Shishkin, Ms. Michelle Sipics, Dr. Sukrit Dasgupta, Mr. Vilas Veeraragahavan, and Mr. Nicholas Vacirca.

The long hours of research and studying were made easier by socializing with friends and colleagues. Mr. Andrew Mrozckowksi, Mr. Eric Gallo, and Dr. Ananth Kini have always lent an ear or given a hand when I was in need. I would especially like to thank Dr. Adam ODonnell, for these reasons and many others. He will laugh at being referred to as a role model, but his example helped guide me through my graduate studies. I thank Mr. Ryan Jung for offering alternative viewpoints and for always being there at the greatest moments of need.

I would like to thank all the members of my Ph.D. dissertation committee, who have donated much of their valuable time in reading my work and hearing my presentations. They have given me indispensable insight and encouragement, while their comments and questions have made my dissertation stronger.

None of my education and scholarly pursuits would have been possible without the support and guidance from my advisor, Dr. Kapil Dandekar. His knowledge,

creativity, and technical ability made great research projects possible and successful. Over the last several years, he helped shape my work and elevate my abilities as a researcher. If it were not for his patience and flexibility, my graduate studies would have been much more difficult. I thank him for never losing faith in me even at difficult times. I look up to his abilities as a teacher and mentor as an invaluable model. Thank you for everything.

Finally, the climb to the end was aided by the support and love of my family. Thank you Mom, Dad, and Emily, for introducing me to scientists in elementary school, waking me to see Haileys comet in the middle of the night, and taking me on my first adventures. Your love and support has been unwavering, whether you were listening to me play concertos or listening to me describe multipath fading.

And last but not least, my dearest Mariah, you helped me put one foot in front of the other through to the end. I love you, and thank you for all of your support.

Table of Contents

Dedications ii

Acknowledgements iii

List of Tables ix

List of Figures x

Abstract xii

Chapter 1. Introduction 1

1.1 Motivation 1

1.2 Outline and Contribution 2

Chapter 2. Background and Tools 4

2.1 Background 4

2.2 Formulation 5

2.2.1 Notation 6

2.2.2 Channel Model 6

2.2.3 Normalization 8

2.2.4 Capacity 8

2.3 Experimental Testbed 9

2.3.1 Analog Front End 11

2.3.2 Physical Layer 13

2.3.3 MAC and Higher Layers 13

2.4 Environment 14

2.5 Simulation Tools 14

Chapter 3. Experimental Analysis of Power Control Algorithms 17
3.1 Introduction 17
3.2 Power Control Formulation 18
3.3 Resource Allocation Strategies 19
3.3.1 Independent Waterfilling 19
3.3.2 Multi-user Waterfilling 20
3.3.3 Gradient Projection Method 21
3.3.4 Game Theoretic Method 21
3.4 Results 23
3.4.1 Link Results 24
3.4.2 Network Capacity 27
3.4.3 Comparison of Measured Convergence Rates 29
3.4.4 Comparison of Simulation and Measurements 32
3.5 Conclusion 33
Chapter 4. Antenna Spacing 34
4.1 Introduction 34
4.2 Network and Channel Models 37
4.2.1 Channel and Interference Model 37
4.2.2 Capacity in Co-channel Interference Limited Networks 37
4.3 Singular Value Analysis 39
4.3.1 Singular Value Metrics 39
4.3.2 Correlation and Sum of Singular Values 41
4.3.3 Balance between Sum and Ratio of Squared Singular Values . 42
4.4 Results 43

4.4.1 Evaluation of Singular Values 44
4.4.1.1 Ratio of squared singular values 44
4.4.1.2 Sum of Squared Singular Values 46
4.4.1.3 Expected Capacity 46
4.4.2 Capacity vs. SINR 51
4.4.3 Crossing Point Level vs. SIR 54
4.5 Conclusions 56
Chapter 5. Optically Transparent Flexible MIMO Antennas 57
5.1 Introduction 57
5.2 Antenna Design 58
5.3 Antenna Fabrication 60
5.4 Antenna Array Characteristics 62
5.5 Flexibility and Transparency 63
5.5.1 Flexibility 65
5.5.2 Transparency 66
5.6 Network Performance 68
5.6.1 MIMO Network Capacity 70
5.6.2 Packet Error Rate 71
5.7 Conclusion 73
Chapter 6. Conclusion 76
Bibliography 78
Appendix A. Table of Symbols 83
Appendix B. Table of Acronyms 84
Vita 85

List of Tables

3.1 Measured Sum-rate Capacity and Effiency for single scenario with SNR=20 dB 27

List of Figures

1.1 Overview of research areas 2

2.1 Multiple antenna network with co-channel interference 7

2.2 Block diagram of the software defined radio measurement testbed . . 11

2.3 Multiple antenna software defined radio measurement testbed 12

2.4 Indoor measurement testing environment and node locations 15

2.5 Visual representation of the simulations with FASANT 16

3.1 The scenario used for measurements and simulations in the Bossone building 23

3.2 Link capacity using independent waterfilling (IWF) technique 25

3.3 Link capacity using multi-user waterfilling (MUWF) technique . . . 26

3.4 Link capacity using the global gradient projection (GGP) technique . 27

3.5 Measured link capacity versus SNR with GT power allocation in the scenario shown in Fig. 3.1. 28

3.6 CDF of sum-rate capacities for different methods from measurements and simulations over all scenarios 29

3.7 CDF of energy efficiencies for different methods from measurements and simulations over all scenarios 30

3.8 CDF of the convergence rates of the power allocation methods from measurements 31

3.9 CDF of the ratio of singular values from measurements and simulations 32

4.1 Ratio of squared singular values vs. number of interferers 45

4.2 Sum of squared singular values vs. number of interferers 47

4.3 Expected sum capacity vs. number of interferers for INR = 10 dB . 49

4.4 Expected sum capacity vs. number of interferers for INR = 20 dB . 50

4.5 Expected capacity vs. signal to interference ratio with 1 interferer for simulated and measured channels with INR={10,20} 52

4.6 Expected capacity vs. signal to interference ratio with 5 interferers for simulated and measured channels with INR={10,20} 53

4.7 Signal to interference ratio crossing point in capacity with INR={10,20} dB for the simulated and measured channels 55

5.1 Chemical diagram of PEDOT(upper)-PSS(lower) 59

5.2 Transparent MIMO antenna array with dilution of 1:2 DI polymer to water 61

5.3 Measured return loss for a copper antenna and a transparent conductive polymer antenna 63

5.4 A comparison of the radiation patterns of a copper and a conductive polymer MIMO antenna arrays 64

5.5 Picture of a conductive polymer antenna with different amounts of bending 65

5.6 A comparison of the radiation patterns of a MIMO conductive polymer antenna array with a decreasing bend in the substrate: $\theta = 180°$, $\theta = 160°$, $\theta = 95°$. 67

5.7 Measured return loss of the conductive polymer antennas with different levels of dilution 68

5.8 A comparison of the radiation patterns of MIMO polymer antenna arrays with a decreasing conductivity: Copper, full strength PH500, 1:1 PH500:H_2O, and 1:2 PH500:H_2O. 69

5.9 Percent of optical transmission through the dipole conductive polymer antenna for: full strength PH500, 1:1 PH500:H_2O, and 1:2 PH500:H_2O 70

5.10 Scenarios used for measurements the MIMO network performance of a conductive polymer antenna array 72

5.11 Link capacity of scenario #1 using MIMO transparent antennas . . . 73

5.12 Link capacity of scenario #2 using MIMO transparent antennas . . . 74

5.13 Link capacity of scenario #3 using MIMO transparent antennas . . . 75

Abstract

Experimental Analysis of Power Control and Element Spacing for Unobtrusive MIMO Antenna Systems
Nicholas J. Kirsch
Kapil R. Dandekar, Ph.D.

With ever-increasing demand for wireless communications, spectral efficiency and power management are of great importance. Mobile nodes in an ad hoc network are limited by the available power, interference, and shared communication resources. Research shows that multiple-input multiple-output (MIMO) communication systems can increase capacity and mitigate interference by exploiting the multi-path nature of wireless energy. This increase in capacity is realized with an array of antennas that can transmit multiple uncorrelated streams. In order to achieve theoretical gains in capacity, several practical problems must be considered. This dissertation presents solutions to create higher quality communication systems in MIMO ad hoc networks through power management, antenna array spacing, and unobtrusive conductive polymer antennas.

To show how co-channel interference can be managed in ad hoc networks, the experimental performance of several power control methods are demonstrated. These experiments were made with a multiple antenna software defined radio (SDR) testbed and verified with electro-magnetic ray tracing. In addition, the spacing between antenna array elements directly impacts the wireless channel. An analysis of the wireless channel is presented to show the impact of the antenna spacing and co-channel interference on the network capacity. A method for selecting the best antenna spacing is also described based upon the channel analysis. Finally, due to the size of mobile devices, it is difficult to incorporate MIMO systems into small form factors. A transparent, conformal antenna array was fabricated to demonstrate that antennas can be developed to fit into small form factors and perform at a high level.

Chapter 1. Introduction

1.1 Motivation

Wireless communications is a broad, rapidly growing technology that impacts the lives of people throughout the world. The driving force behind the demand for better wireless communications is mankind's inherent need to communicate. Over the past sixty years, our greater understanding of physical fundamentals of electromagnetism has enabled easier and more reliable communications [1,2]. Coupled with the increases in computational power of micro-electronics, mobile wireless communication systems have infiltrated people's lives [3]. With ever increasing demand for more reliable communications, engineers are continually investigating better and faster ways for people to communicate in the face of physical fundamental limits and to more easily integrate communication systems into everyday life.

There are many limiting factors to wireless communications, but one of the most detrimental limiting factors is interference. Interference is caused intentionally or unintentionally by nodes in a network or by other sources of electromagnetic energy. Interference is the physical limitation of spectrum availability. A very popular and well researched topic for increasing spectral efficiency and mitigating interference is multiple-input multiple-out (MIMO) communications.

There is a large amount of research in the area of multiple antenna communications (See Ch. 2). This research shows how data rates can be improved by adding multiple antennas to transmitters and receivers. Due to the scarcity of wireless spectrum, nodes in a network need to share spectrum, which also makes them relevant to study. However, there is limited research on testbeds describing actual MIMO network systems.

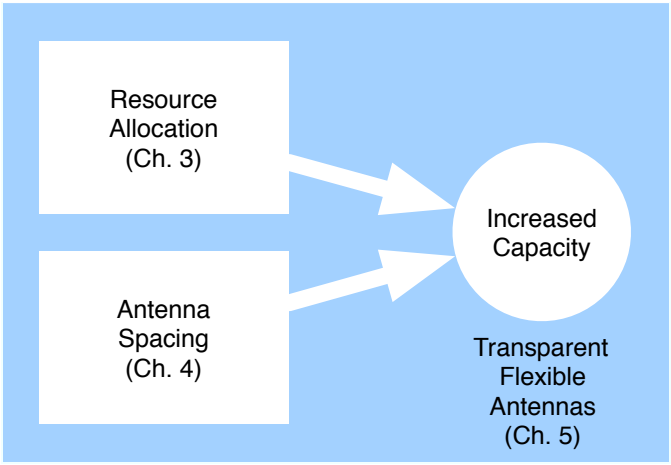

Figure 1.1: Overview of research areas

With an array of antennas, wireless communications capacity can be increased by intelligent use of power and design of the antenna systems. Figure 1.1 illustrates how each contribution in this dissertation fits together. Experimental results demonstrate how the capacity of multiple antenna communications systems can be increased with power control in an ad hoc network (Ch. 3) and by proper spacing of the antenna elements (Ch. 4). Additionally, there are cases when the dimensions of the antenna array make it prohibitively difficult to incorporate antenna arrays into a particular form factor, such as very large or small spacings. Therefore, there is a necessity to have technologies to enable antennas arrays to be unobtrusive, such as transparent flexible antennas (Ch. 5).

1.2 Outline and Contribution

Chapter 2 presents greater background on MIMO communications and a survey of previous work. Because much of this dissertation is based upon measurements, detailed information on the simulation tools used and software defined radio testbed are provided.

Chapter 3 describes the results of the first measurement campaign on power allo-

cation in MIMO communication systems [4, 5]. The experimental results show that different allocation strategies increase network capacity in a wireless network. An experimental comparison of several methods shows the trade-off between centralized versus decentralized decision making and the amount of network status knowledge needed to increase capacity.

Chapter 4 shows how the spacing between antenna elements in an array affects the network capacity in a network setting [6]. Previous, single link research has shown that wider spacing increases capacity. However, this antenna spacing conclusion does not necessarily apply to links operating with co-channel network users. A method for calculating capacity to include antenna spacing is presented in this chapter. Further, if the network parameters identified by this analysis can be anticipated by a designer, the optimal antenna spacing can be determined before deployment.

Finally, Chapter 5 presents novel transparent antennas made from conductive polymers [7, 8]. These antennas are also conformal and flexible, which make them suitable for a wide range of situations. One of the impediments to deploying MIMO systems is that antennas arrays cannot be unobtrusively placed. Transparent, conformal, antenna technology discussed in this dissertation can be can enabling technology in increasing the prevalence of MIMO communications systems. This chapter includes information on the design, transparency, and flexibility of the antennas. Further, network capacity results using the conductive polymer are presented.

Chapter 2. Background and Tools

This chapter provides background information necessary to understand the research presented in the later chapters of this dissertation. The subsequent chapters all utilize similar theoretical formulations, which are presented here and then elaborated on in later chapters as different aspects of MIMO communications are studied. Because of the experimental nature of the research presented, details on the hardware and simulations tools are provided.

2.1 Background

To increase spectral efficiency, Multiple-input multiple-output (MIMO) communication systems use an array of antennas at both ends of a communications link. The spatial diversity of the antennas can exploit the lack of correlation between the different pairwise channels in transmitting and receiving arrays, which can increase the communications rate or capacity [9]. When channels are uncorrelated, multiple streams of information can be transmitted over an array of antennas. However, spatial separation and the channel response are closely related [10]. There has been a large amount of published research which shows significant capacity gains that can be achieved by using antenna arrays [9, 11, 12]. By studying the correlation of the antenna spacing and the communication channel, we can gain insight to achieving higher capacity.

For a single communications link, it is straight forward [13] to find the best way to allocate power to achieve the highest capacity. However, in a co-channel network, the problem becomes more complicated [14,15]. Power management in ad hoc networks is important because of changing link conditions and user requirements. Without some

supervisory system in an ad hoc network, nodes would be prone to allocate power as they see fit. Previous work describes [16] decentralized methods to allocate power per node and to increase capacity. Power allocation in both MIMO systems and ad hoc networks depend closely on the sensing of the channel and then acting to benefit the user. If MIMO communications with ad hoc power allocation and antenna spacing techniques are combined, networks would have a vast improvement in transmission flexibility and spectral efficiency.

Through the experimental demonstration of MIMO power allocation schemes, we will observe that the antenna spacing has a great affect on the capacity of the system. Because capacity is dependent on the link-of-interest and all the of co-channel interfering links, one must consider the effect of antenna spacing in all network nodes [17]. A major contribution of this dissertation is to show how spacing effects sum-rate capacity and how a network designer could decide on antenna spacing before or during the deployment.

Methods placing radios and antennas systems into smaller form factors is also important for wireless communications to be more seamlessly incorporated into people's lives and still meet the demands of greater capacity. Antenna systems that can conform to a particular surface or are transparent make this possible. There has been research into this area to make antennas out of non-metallic materials [18], which makes them transparent. However, most of these materials are not necessarily conformal or flexible.

2.2 Formulation

The next few chapters will present the theory and results from different aspects of MIMO communications, which all share a similar framework. This framework is provided along with multiple antenna communication systems performance measures.

2.2.1 Notation

In this dissertation, a vector is notated as $\mathbf{a}$ and a matrix is $\mathbf{A}$. The conjugate transpose is denoted as $\mathbf{A}^{\dagger}$, $\mathrm{Tr}(\mathbf{A})$ denotes the trace, and $\det(\mathbf{A})$ denotes the determinant if $\mathbf{A}$ is square. An identity matrix is $\mathbf{I}_N$, where N is the number of rows and columns. The expectation of a matrix is $E\{\cdot\}$.

2.2.2 Channel Model

In MIMO communication systems, it is important to understand how the wireless channel effects the quality of the communications link. Further, it is also important for a communications engineering to understand what forces, e.g. interference, scatterers, etc., affect the channel. Therefore, we first consider a simple model for the communications channel. The communication model consists of an input signal from a transmitter with N_t antennas, a wireless channel with complex gain, noise, and a received signal or output vector from a receiver with N_r antennas. For some link l, the received signal vector $\mathbf{y_l}$, which has dimension $N_r \times 1$ is

$$\mathbf{y_l} = \mathbf{H}_{l,l}\mathbf{x}_l + \mathbf{n}_l. \tag{2.1}$$

The transmitted signal, $\mathbf{x_l}$, is a vector of size $N_t \times 1$. The complex channel gain, or simply channel, $\mathbf{H}_{l,l}$ between receiver and transmitter of the l^{th} link is a $N_r \times N_t$ matrix. Finally, $\mathbf{n}_l$ is the Gaussian background noise.

Most of this research studies networks that are limited by co-channel interference links and therefore we must consider the interference channels from these links. For a network of interest, there are $\mathcal{L} = \{1, 2, \ldots, L\}$ links and each link receives interference from the other links.

An example network can be seen in Fig. 2.1. In this example, the link of interest is blue and has an arrow from the transmitter to the receiver. Each node in the network

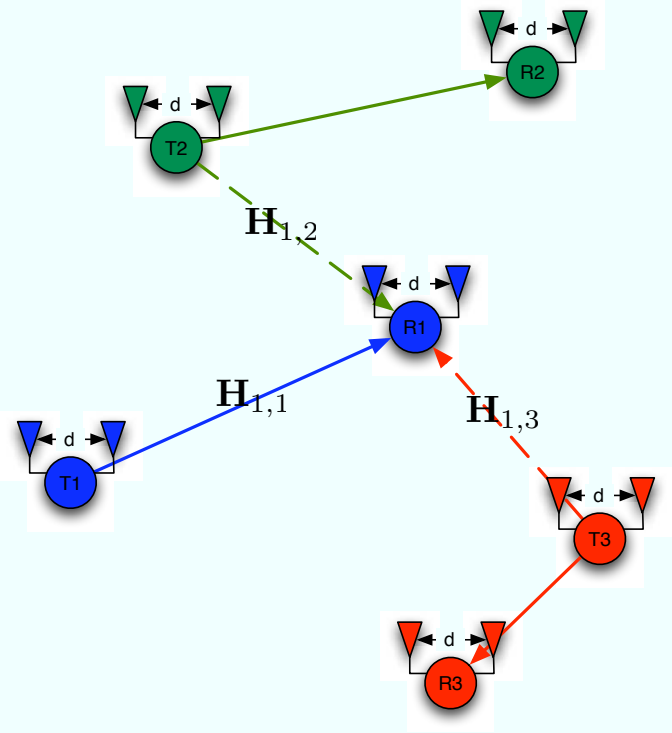

Figure 2.1: Multiple antenna network with co-channel interference

has two antennas which form a linear array and have a spacing of d. The co-channel interference incident upon the receiver of the link of interest from the green and red (interfering) links are dashed lines.

Now, the signal model (2.1) is extended to include the presence of interference of co-channel interference. For a particular link, l, the received signal with interference is

$$\mathbf{y_l} = \mathbf{H}_{l,l}\mathbf{x}_l + \sum_{j=1,j\neq l}^{L} \mathbf{H}_{l,j}\mathbf{x}_j + \mathbf{n}_l, \tag{2.2}$$

where $\mathbf{H}_{l,j}$ is the channel between the receiver in the link of interest l and the transmitter of the interfering link j.

2.2.3 Normalization

To analyze the results of the channel measurements and remove the effects of path loss, the following scaling factor for link l was found by (2.3). The channel sounding testbed described in Sec. 2.3 uses orthogonal frequency division multiplexing (OFDM), which separates the wide bandwidth channel into narrowband subcarriers. This modulation reduces the effect of fading on capacity [19]. The normalization a_l is found with the Frobenius norm of a link l, over all K subcarriers.

$$a_l = \frac{1}{K} \sum_{k=1}^{K} \|\mathbf{H}_{l,l}^{(k)}\|_F^2 \tag{2.3}$$

Once k_l is found for all L, the median k_l was selected making the normalization factor,$\sqrt{\frac{a_l}{N_t N_r}}$, which was then applied to all $\mathbf{H}_{l,l}^{(k)}$ and $\mathbf{H}_{l,j}^{(k)}$. This normalization maintains the relative strength between the desired link and interfering channels.

2.2.4 Capacity

An important measure of the performance of a MIMO system is the link and system capacity. The capacity of a link is determined by maxmizing the mutual information [13]. For a single MIMO link l, the capacity in bps/Hz is

$$C_l = \log_2 \det(\mathbf{I} + \frac{\text{SNR}}{N_r} \mathbf{H}_{l,l} \mathbf{H}_{l,l}^{\dagger}). \tag{2.4}$$

The single link capacity is a function of the signal-to-noise ratio, the number of antennas and the wireless channel. An important fact to consider is that as the channel matrix $\mathbf{H}$ becomes more "white," or as the rank of the matrix increases, the capacity also increases [9]. Therefore, to increase capacity in MIMO systems, uncorrelated channels, or matrices with high rank are desirable [17].

When a link of interest is in the presence of co-channel interference, the capacity is

now a function of the channels of the interfering nodes. To capture the impact of the co-channel interference and noise, the covariance matrix of the interference-plus-noise is expressed as

$$\mathbf{R}_l = \mathbf{I} + \sum_{j=1, j\neq l}^{L} \mathbf{H}_{l,j}\mathbf{H}_{l,j}^{\dagger}. \tag{2.5}$$

The interference-plus-noise covariance matrix can have a significant impact on capacity, which is investigated further in Ch. 4. The single link capacity, with co-channel interference, is a function of the *inverse* of $\mathbf{R}_l$ and is expressed as

$$C_l = \log_2 \det(\mathbf{I} + \mathbf{H}_{l,l}\mathbf{H}_{l,l}^{\dagger}\mathbf{R}_l^{-1}). \tag{2.6}$$

Finally, the sum-rate or network capacity is the sum of the capacity of the $\mathcal{L}$ links

$$C = \sum_{l=1}^{L} C_l \tag{2.7}$$

The equations for the signal model and capacity are modified in the following chapters as different aspects of MIMO communication systems are explored. In Ch. 3, the transmit signal vectors are changed to reflect control over the transmitted power. Chapter 4 details how the singular values of the wireless channels (2.2) and (2.5) can be used for effective network design. Chapter 5 uses these equations to evaluate the capacity in a network with unobtrusive antennas arrays.

2.3 Experimental Testbed

One important factor in this dissertation is the experimental results that verify the theory and accepted simulation tools. A multiple antenna testbed was built in order to perform experimental measurements for this dissertation. The testbed was designed to be flexible in hardware and software so that a wide range of applications

could be studied. Software Defined Radio (SDR) allows for the implementation of highly flexible communication nodes that are able to use multiple protocol standards on the same physical hardware. There are three main components of the experimental testbed: an analog front end that can include an antenna arrays and a frequency agile RF transceiver, the analog to digital conversion system which includes modulation/demodulation, and the medium access control (MAC). Analog signals are converted to and from digital using PXI data acquisition cards from National Instruments and then passed to a dedicated processor that runs the physical layer (PHY), which is implemented in LabVIEW. This system is designed to provide an easy to implement, easy to modify design that allows maximum experimentation with both the physical layer and the networking software.

The nodes were created at the Drexel University Wireless Systems Laboratory in collaboration with the University of Texas - Austin Wireless Networking & Communications Group. Figure 2.2 shows a basic block diagram of our system and Fig. 2.3 shows an image of one of the testbed nodes. Each of the components is discussed below, but it is useful to first understand how they interconnect. The analog front ends and PHY are all contained in a PXI chassis from National Instruments. Analog signals are converted to and from digital signals using PXI data acquistion cards from National Instruments and then passed to a dedicated processor that runs the PHY, which is implemented in LabVIEW. This processor then communicates over gigabit ethernet with a general purpose host which runs the MAC, higher layer network protocols, and any application software. Note that this design is not intended to provide a high performance physical link, since doing so would require using application specific digital signal processing. Instead, it is designed to provide an easy to implement, easy to modify design that allows maximum experimentation with both the physical layer and the networking software.

The measurement campaigns performed in most of this research study the wireless

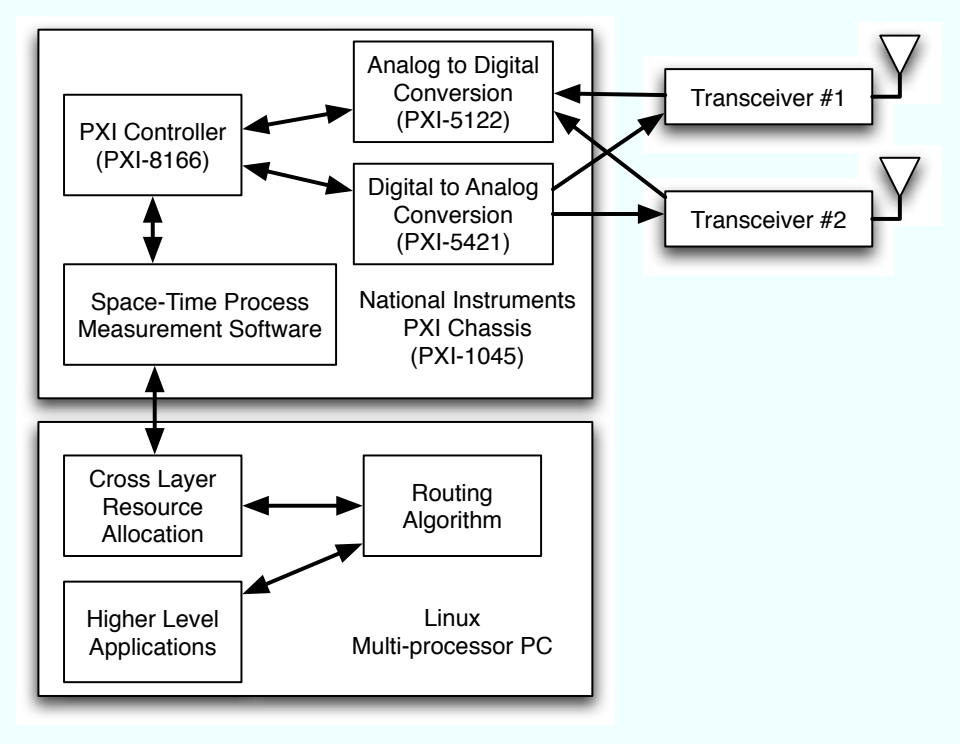

Figure 2.2: Block diagram of the software defined radio measurement testbed

channels. MIMO channels are measured by transmitting a known signal from each of the antennas in the transmit array and then determining the complex channel gain at the receiver. In the following chapters, details on how the measurements were performed are detailed.

2.3.1 Analog Front End

The RF transceivers used in our MIMO SDR testbed – donated by Texas Instruments – are capable of transmitting at all channels in the 2.4 GHz and 5 GHz bands. The radios include low noise/power amplifiers and mixers, but no modulation and demodulation circuits. This front end allows us to create our own software modulation/demodulation so that the testbed operates independently of existing wireless standards, and thus provide us with maximum flexibility.

In this dissertation, the measurements were taken at a center frequency of 2.484

Figure 2.3: Multiple antenna software defined radio measurement testbed

GHz on a BPSK signal with 5 MHz bandwidth. OFDM modulation is used with 64 subcarriers. The baseband processing is based upon the 802.11g standard with modifications to use space division multiplexing (SDM) mode. Specifically, the preamble of the standard (channel training) was used for capturing the channel. Unless otherwise noted, the antennas used for the measurements are omni-directional MAXRAD 6 dBi antennas. The spacing of the antennas in the array are explained in each subsequent chapter.

2.3.2 Physical Layer

Analog/Digital conversion, baseband modulation, demodulation, and post processing are done with a National Instruments PXI-chassis running LabVIEW. NI PXI-5421 cards perform the digital-to-analog conversion at 100 MS/s. Additionally, NI PXI-5122 cards are used for the analog-to-digital conversion at 100 MS/s. Custom code was developed in collaboration with the University of Texas-Austin for modulation and de-modulation. Software was also written to communicate with the upper level layers via ethernet. The custom protocol was written not only for data transfer between layers, but also to allow for flexibility in the implementation of cross-layer protocols.

The radio transceivers we use have independent local oscillators. To counter the offset in phase of due to the independent oscillators (not the offset due to the multipath), we perform an FFT of the received signals and shift one of the signals to compensate for the difference.

2.3.3 MAC and Higher Layers

Although some link functionality (such as framing) is done as part of the PHY, the majority of the MAC and of the higher layer processing is done on a general purpose host computer. We use a dedicated ethernet connection as a dedicated bus to provide communication between the PHY and upper layers.

In implementing the networking software, our goal was to provide maximum flexibility for experimentation. In particular, we based our implementation on the Click Modular Router [20]. Click is well suited to this task, it allows users to write "elements" in C++ that implement base functionality and to glue them together using the Click language. Click can run the resulting configurations at user level or as part of a kernel module resident in the Linux kernel, giving a tradeoff between ease of

development and performance.

2.4 Environment

Our measurement campaign took place in the 3rd floor of the Bossone building on the campus of Drexel University. The floor plan for our measurement environment is shown in Fig. 3.1. The chosen node locations allows for a mixture of LOS and NLOS measurements at various distances between nodes. The antenna arrays are all oriented vertically with respect to the floor.

Two nodes (one transmitter and one receiver) were used to create a simulated multi-node scenario, from which many different scenarios can be constructed. The two nodes were positioned at each Tx and Rx position where 100 channel snapshots were measured. The links used in the single scenario analysis are shown with lines from the transmitter to an arrow denoting the receiver. For example, the channel from Tx:1 to Rx:7 was measured and then the channel from Tx:1 to Rx:8. From these Tx and Rx positions, 720 six-node scenarios are considered in the analysis. In our experiments, we wanted to measure the wireless channel as a function of the building and radio systems, not channels that are affected by short-term fading (e.g. people walking by). During the channel measurements, we tried to keep the environment as stable as possible by limiting the number people from opening doors entering the area of the measurements. After the channels were recorded, the results were calculated off-line.

2.5 Simulation Tools

Computational electromagnetic simulations are used to study the wireless channels, which help validate our experimental results. These simulations calculate the received electromagnetic fields due to all of the multipath rays between every transmitter and

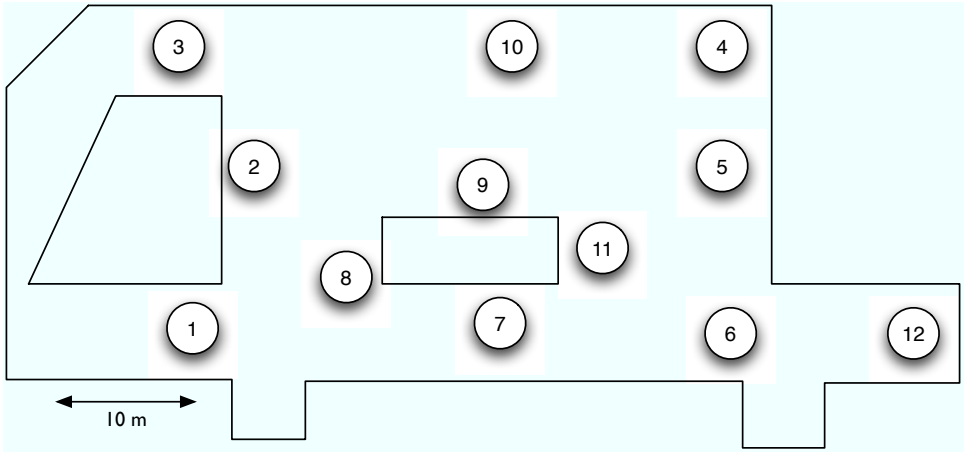

Figure 2.4: Indoor measurement testing environment and node locations

every receiver. To simulate an indoor environment to determine the performance of the different power allocation methods, the ray tracing program FASANT [21, 22] was used with a 3-D model of the Bossone environment. The 3-D indoor model includes all major walls and floors using relative permittivity and permeability for those objects: $\epsilon_r = 4.44, \mu_r = 0.99$ and $\epsilon_r = 3, \mu_r = 0.99$ respectively. Only major features were included and no additional scattering bodies were in the simulation environment. Simulations were run at a frequency of 2.484 GHz at the same locations as in the measurements. Figure 2.5 shows an example rendering of the solution for one simulation of FASANT with two nodes. The white symbols represent the nodes and the red lines are the calculated rays. The multi-path rays are then summed to find the wireless channel

The antenna arrays were modeled as dipoles in the simulation package FEKO [23]. Radiation patterns for these near field simulations were used as an input to FASANT. We have previously used this simulation scheme to simulate MIMO network links [4, 16] At each location, simulations were performed in a 10×10 grid of positions with separation $\lambda/10$. The channel response from this grid of positions was used to provide local averaging to reduce the effects of small scale fading. The simulated channels were also normalized with the same procedure as the measurements detailed

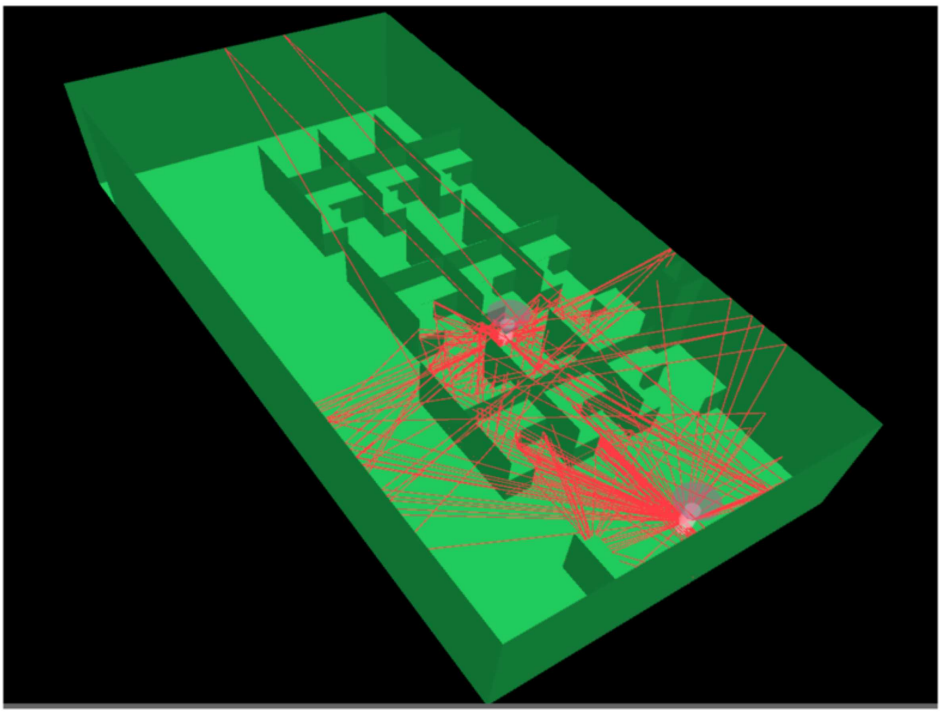

Figure 2.5: Visual representation of the simulations with FASANT

in Sec. 2.2.3.

Chapter 3. Experimental Analysis of Power Control Algorithms

3.1 Introduction

Multiple input multiple output (MIMO) systems have proven to be very promising for increasing spectral efficiency of ad-hoc networks [9]. Efficient use of frequency and power is an important goal of any resource limited system. Recent work has shown that these systems can have increased capacity through improved power control. Power control, or resource allocation, is accomplished by assigning power to eigenmodes of the MIMO matrix channel that provide the best capacity. In an interference free system, the optimal solution is independent waterfilling (IWF) [13].

At the expense of network overhead and computational complexity, sophisticated power allocation methods can be used to increase system capacity by limiting external interference, such as multi-user waterfilling (MUWF) and the global gradient projection method (GGP) [14]. MUWF improves capacity by channel whitening. The GGP method improves capacity by globally calculating power to determine the best power allocation. Recent work has been published that takes a game theoretic (GT) approach to the resource allocation problem [4]. This iterative and distributed technique has been shown to outperform MUWF and approach the performance of GGP using energy efficiency and capacity as a metric [16].

While experimental characterization has been performed on the MUWF and GGP techniques [4], the purpose of this chapter is to show experimental results for the GT method and compare them with the other techniques and simulations in a similar environment. Further, a comparison of the measured results and simulations is provided. With these experimental findings, a greater understanding can be achieved into the impact that power allocation has on the capacity in ad hoc networks.

In the following section, the system model (2.6) is modified to take into consideration power control. The power control algorithms are presented in Sec. 3.3. The results are shown in Sec. 3.4 with a description of the simulations, measurements, and experimental scenario.

3.2 Power Control Formulation

In this chapter, the goal is to show different methods that control the power transmitted at each node in a network that is limited by co-channel interference. The transmitted power can be controlled by adjusting the transmitted signal vector $\mathbf{x_l}$ of the multi-link signal model (2.2). The transmitted signal $\mathbf{x}_l$ has the covariance matrix $\mathbf{Q}_l = E\{\mathbf{x}_l\mathbf{x}_l^\dagger\}$. $\mathbf{Q}_l$ is the power allocation matrix and the transmit power for link l is given by $\mathrm{Tr}(\mathbf{Q}_l)$. By adjusting the transmit signal, the amount of power transmitted on each mode can be adjusted. Therefore, the instantaneous data rate of link l (2.6) is now a function of the power allocation matrix.

Because the capacity of a link of interest (2.6) is function of the channels of the co-channel interferers, the capacity is also a function of the power allocation matrices of the co-channel interferers $\mathbf{Q}_j \mathrm{for} j = 1 \ldots \mathcal{L}, j \neq l$. The capacity for a link of interest l is now

$$C_l(\mathbf{Q}_1, ..., \mathbf{Q}_L) = \log_2 \det(\mathbf{I} + \mathbf{H}_{l,l}\mathbf{Q}_l\mathbf{H}_{l,l}^\dagger\mathbf{R}_l^{-1}). \tag{3.1}$$

To capture the impact of the co-channel interference and noise, the covariance matrix of the interference-plus-noise (2.5) is now expressed as

$$\mathbf{R}_l = \mathbf{I} + \sum_{j=1, j\neq l}^{L} \mathbf{H}_{l,j}\mathbf{Q}_j\mathbf{H}_{l,j}^\dagger. \tag{3.2}$$

$\mathbf{R}_l$ is a function of the sum of interfering links. The sum-rate capacity (2.7) can be determined by

$$C(\mathbf{Q}_1, ..., \mathbf{Q}_L) = \sum_{l=1}^{L} C_l(\mathbf{Q}_l) \tag{3.3}$$

The capacity for a given network will vary depending on the method that each link calculates $\mathbf{Q}_l$. For example, a simple power allocation is $\mathbf{Q}_l = \frac{P}{N_t}\mathbf{I}$, which is the total power, P, distributed equally over N_t antennas. The next section goes into further detail on the allocation methods used in the analysis.

3.3 Resource Allocation Strategies

There are several strategies considered in this section to allocate power to antennas (i.e. set $\mathbf{Q}_l$ for link l) in a MIMO ad hoc network. These techniques vary in performance and have different computational and network overhead requirements.

3.3.1 Independent Waterfilling

For a single MIMO link, l, assuming only local channel knowledge and neglecting the effect of interference (i.e., $\mathbf{R}_l = \mathbf{I}$), the optimum signaling problem is to find the optimum $\mathbf{Q}_l$ to maximize $C_l(\mathbf{Q}_1, ..., \mathbf{Q}_L)$ in (3.1). This optimization can be achieved by using the "independent water-filling" (IWF) approach [13].

This allocation is found first by determining the eigenvalue decomposition of the channel of the link of interest. For simplicity, the link subscript is not included in this subsection.

$$\mathbf{H}\mathbf{H}^{\dagger} = \mathbf{V}\mathbf{\Lambda}\mathbf{V}^{\dagger} \tag{3.4}$$

where $\mathbf{V}$ is a unitary matrix and $\mathbf{\Lambda}$ is a diagonal matrix of the eigenvalues. The optimal power allocation is

$$\mathbf{Q} = \mathbf{V}\left(\mu\mathbf{I} - \Lambda^{-1}\right)\mathbf{V}^{\dagger} \tag{3.5}$$

Given some total power limit per node, the "water level" is μ which is chosen to satisfy $\mathrm{Tr}(\mu\mathbf{I} - \Lambda^{-1})^{+} = P$. Therefore, IWF essentially maximizes the capacity for its own link. In comparison to the other MIMO power control algorithms, this technique has the smallest computational complexity and incurs little network overhead. However, independent water-filling does not account for interference effects, which greatly limits its performance in the presence of interference.

3.3.2 Multi-user Waterfilling

If we assume that a transmitter of link l is aware of the interference environment in which the link is operating, the IWF method can be improved. The improvement comes at the cost of higher networking overhead. Specifically, this improvement assumes that the receiver of link l estimates $\mathbf{R}_l$ and instantly relays this information back to the transmitter of link l. The IWF approach is modified to incorporate this interference information by "whitening the channel matrix" first [24,25]. Specifically, application of a spatial whitening transform [15] to the channel yields

$$\tilde{\mathbf{H}}_{l,l} = \mathbf{R}_l^{-1/2}\mathbf{H}_{l,l}. \tag{3.6}$$

Substituting $\mathbf{H}_{l,l}$ in (3.1) with the whitened channel $\mathbf{H}_w$, the multiuser water-filling (MUWF) capacity for link l is calculated. Similar to the IWF method, this method calculates the power allocation matrix distributively and maximizes its own capacity. However, the difference is each link now maximizes its own capacity based upon the interference received from other links.

3.3.3 Gradient Projection Method

The next resource allocation method aims to maximize $C(\mathbf{Q}_1, ..., \mathbf{Q}_L)$ in (3.3), which is the social optimum for the network. This is different from MUWF and IWF because the algorithm seeks to maximize the capacity of the entire network, not just individual links. Therefore, this method requires centralized control in order to increase the capacity compared to the other methods.

To achieve optimum system capacity, the transmitters of each link must cooperate when deciding their power allocation matrices. A compromise is struck between the maximization of an individual links mutual information and the minimization of the interference observed by other users. The global gradient projection (GGP) method, which is an extension of the unconstrained steepest descent method in convex constrained optimization problems, is a technique that can be used solve this social optimum problem [14].

The centralized controller for the GGP method must have access to all channel state information and covariance matrices for all users. This controller performs the calculation and sends the information to all users so that they can update their power allocation matrices accordingly. The GGP technique has the largest networking overhead and has the greatest computational complexity in order to find the optimal allocation of resources.

3.3.4 Game Theoretic Method

The game theory power allocation method is a distributed system where each "player," or link, controls its power based upon the utility (i.e. capacity) of a link and a penalty function for transmitting power. The utility of a link is the link capacity, C_l, which is a function of the squared singular value of the whitened channel, $\sigma_{i,i}$. The penalty or pricing function is then a function of the amount of power a link uses, P_l, to prevent a

link from transmitting unnecessarily high power. P_l is scaled by a pricing factor γ_l to enforce a minimum capacity per unit power. Therefore, the net-utility function can be expressed as, $u_l = C_l - \gamma_l P_l$. With this net-utility function, the per-link objective function can be expressed as

$$\max_{\mathbf{z_l}} \sum_{i=1}^{N_t} \log_2(1 + p_{l,i}\sigma_{l,i}) - \gamma_l \sum_{i=1}^{N_t} p_{l,i} \tag{3.7}$$

such that $\sum_{i=1}^{N_t} p_{l,i} \leq P_l$, which is the total power constraint. Further, the value of γ_l, must be selected. Details for computing γ_l are described in [16] along with the complete details of how links can be shutdown completely if their capacity does not exceed a pre-specifed threshold. In this chapter, a "soft shutdown" mechanism is used for γ_l. This mechanism sets γ_l such that most links use less than maximum power.

Quantitatively, the MUWF and GT methods are similar in that they both maximize the capacity of each user, which means that the power covariance matrix for each user is of the form $\mathbf{Q}_l = \mathbf{V}_w \mathbf{\Lambda} \mathbf{V}_w^H$, where $\mathbf{V}_w$ comes from the SVD of the *whitened channel matrix*, $\mathbf{H}_w = \mathbf{R}^{-1/2}\mathbf{H} = \mathbf{U}_w \mathbf{\Lambda}_w \mathbf{V}_w^H$. Notice that the whitened channel matrix per user can be different for MUWF and GT, since some links are shutdown and transmitted power per link is different even though they start with the same total available power.

In the GGP method, the objective is no longer to maximize the capacity of each user, but rather to maximize the sum capacity of the network. Therefore, the eigenvectors of $\mathbf{Q}_l$ no longer coincide with the right unitary matrix of the SVD of the whitened channel matrix. This occurs because the choice of optimal $\mathbf{Q}_l$ per user is affected, not only by the resulting single user capacity, but also by interference imposed to others via the interference plus covariance matrix ($\mathbf{R}_l$). Thus, the eigenvectors that find a "sweet spot" between the two objectives (single user capacity and interference imposed on other users) are used. These eigenvectors are usually different from the

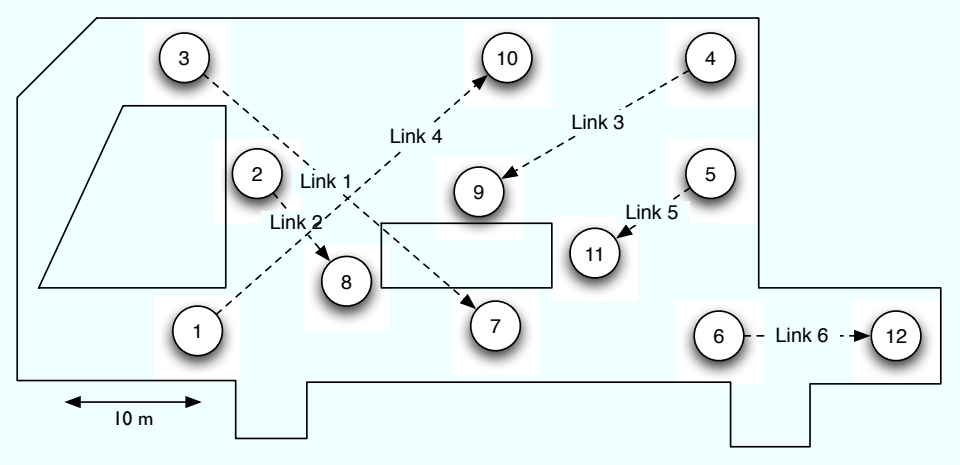

Figure 3.1: The scenario used for measurements and simulations in the Bossone building

eigenvectors of the whitened channel matrix.

3.4 Results

The simulations and measurements used to find the results are described in Ch. 2. With the simulation and measurement tools many different scenarios are analyzed. First, the links are used to measure a single scenario shown with lines from the transmitter to an arrow denoting the receiver as in Fig. 3.1. Second, from all of the Tx and Rx positions, 720 six-node scenarios are considered in the multi-scenario analysis. Therefore, we present the performance of the different power allocation methods for a single scenario of interest and every possible six node scenario. There are two antennas at each node with a spacing of $\lambda/2$.

After the channels were recorded, the three different power allocation methods were used to calculate the capacity off-line. The total power available for each link was initialized to 20 dB. For each scenario, the instantaneous capacity was calculated for the 100 snapshots. In a real-time wireless communication system, once all the channels were determined at the receiver of a particular link, the channels would be sent to the transmitter which would then calculate power allocation.

3.4.1 Link Results

Once the channel measurements were taken, the different power allocation techniques from Section 3.3 were evaluated first by comparing the measured link capacity for one scenario of interest (out of the 720 possible six-node scenarios), for increasing values of SNR

Figure 3.2 shows IWF capacity performance of all links versus SNR in an interference limiting environment. Each node makes a decision on power control based upon knowledge of only $\mathbf{H}_{l,l}$, the link's own channel state. Link 6 has the highest capacity, which can be attributed to the fact that the receiver of that link is isolated from the other transmitters. Additionally, the capacity of the other links at higher SNRs is lower due to the the interference created by Link 6. This is due to favorable channel conditions and equal transmission powers. This allocation method has the lowest capacity because each link is determining the best power allocation for itself, without accounting for interference.

Figure 3.3 shows the capacity of all links versus SNR for the MUWF allocation method. The calculated capacity flattens because as SNR increases for the link of interest, the interference also increases. Link 6 has much greater capacity than the other links because the receiver is affected minimally by the other links. In comparison with the IWF allocation, the links have similar relative performance. Links 4 and 1 have low performance due to the presence of many other transmitting nodes.

The results from the GGP method can be seen in Fig. 3.4. Overall, there is higher capacity in comparison to the MUWF. However, to achieve higher rates links 1 and 4 are nearly "shut down" to limit the amount of interference they generate. Both links are long-distance and cause unnecessary interference to the rest of the network. As is the case, with the other allocation methods, Link 6 has the best performance. Additionally, there is a crossing in the capacity of Links 2 and 5 as

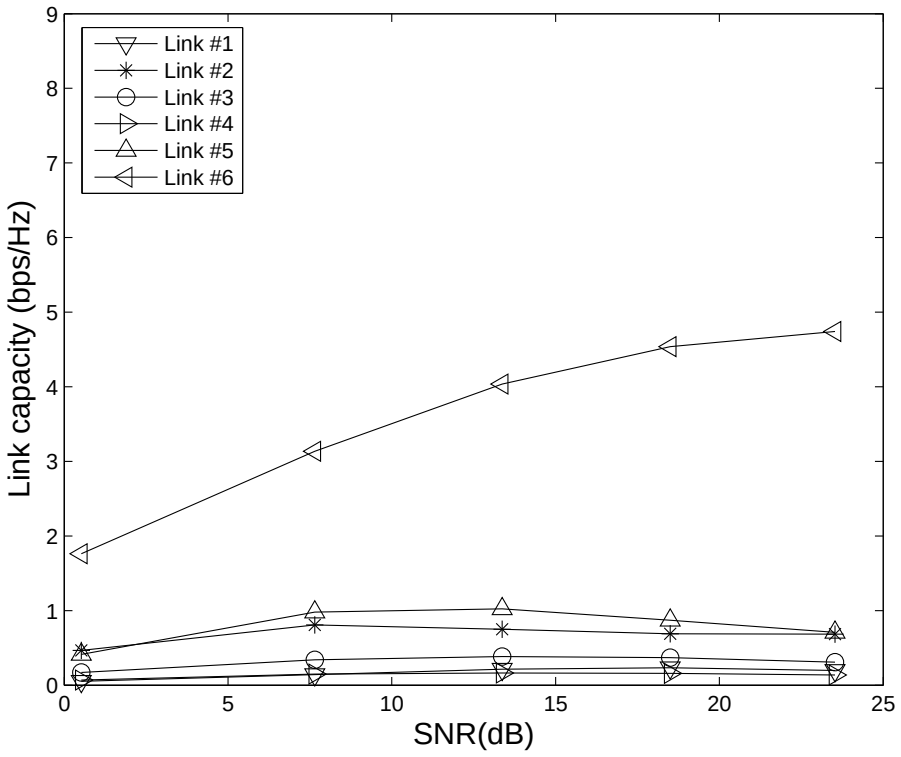

Figure 3.2: Link capacity using independent waterfilling (IWF) technique

SNR increases. This crossing occurs due to the interference created by Link 2, which limits the capacity of other links that have higher rank channel conditions.

Finally, the link capacity results of the game theory method are presented in Fig. 3.5. From the chosen scenario (Fig. 3.1), one can see how these capacities are achieved. First, because link 6 is more isolated than the other links, the receiver is less affected by other transmitters. The transmitter of link 6 has little effect on the other receivers. Therefore, more capacity can be achieved by the channel that has little interference. Both links 1 and 4 are susceptible to greater sources of interference and would not yield much capacity without greater signal power. Therefore, these links are shut-down to prevent unnecessary interference to the rest of network. Links 5 and 2 are similar to each other and are moderately affected by interfering links because the receivers of these links are in a centralized location. Last, link 3 is able

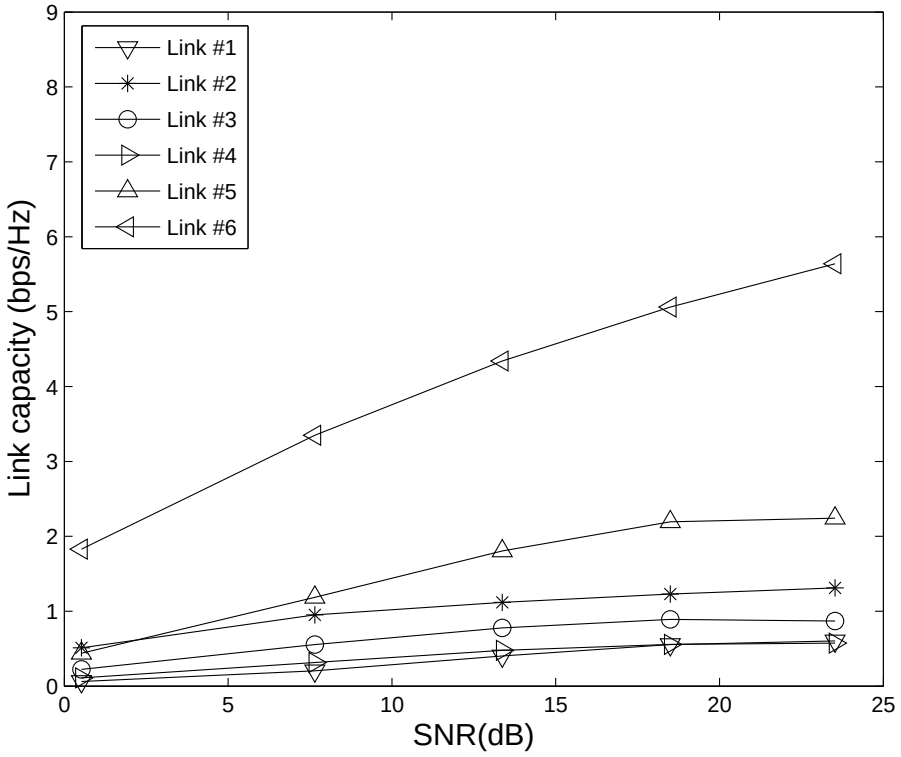

Figure 3.3: Link capacity using multi-user waterfilling (MUWF) technique

to achieve a relatively small level of capacity amidst the co-channel interference.

Table 3.1 is the comparison of the measured sum-rate capacity and the efficiency results from this scenario using different power allocation schemes. The energy efficiency λ, is the ratio of the network capacity to the total network power (bps/Hz/W). With 20 dB of SNR, GT has a sum-rate capacity between MUWF and GGP. However, this specific scenario is an example of the GT method providing higher efficiency than the GGP method. This condition occurs due to the GT method using lower transmit powers. These results match the interpretation that GT is an improvement over MUWF. The GGP method is able to achieve greater capacity due to its use of greater levels of network information (and overhead).

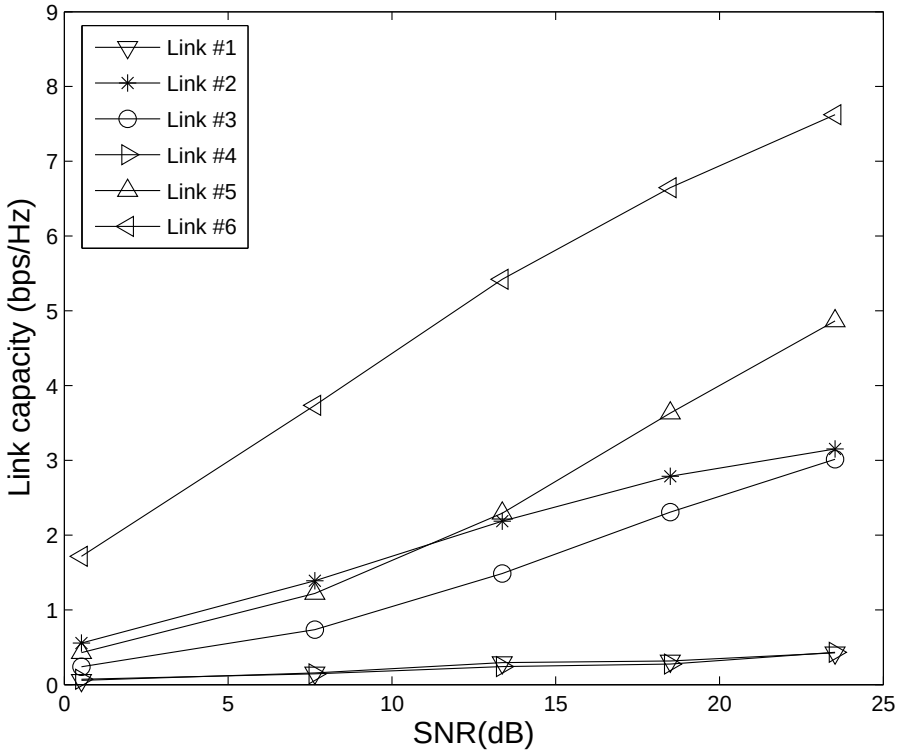

Figure 3.4: Link capacity using the global gradient projection (GGP) technique

Table 3.1: Measured Sum-rate Capacity and Effiency for single scenario with SNR=20 dB

Allocation scheme	Capacity (bps/Hz)	Efficiency
MUWF	11.56	0.0193
GGP	16.52	0.0275
GT	13.22	0.0314

3.4.2 Network Capacity

Next, with 720 six-link scenarios and data from 100 locations and snapshots from simulations and measurements respectively, the sum-rate capacity was calculated and the cumulative distribution function (CDF) for the three resource allocation schemes is shown in Fig. 3.6. The capacity for GT is higher than the MUWF case, however not as high as the GGP method. The GGP method assumes a centralized control

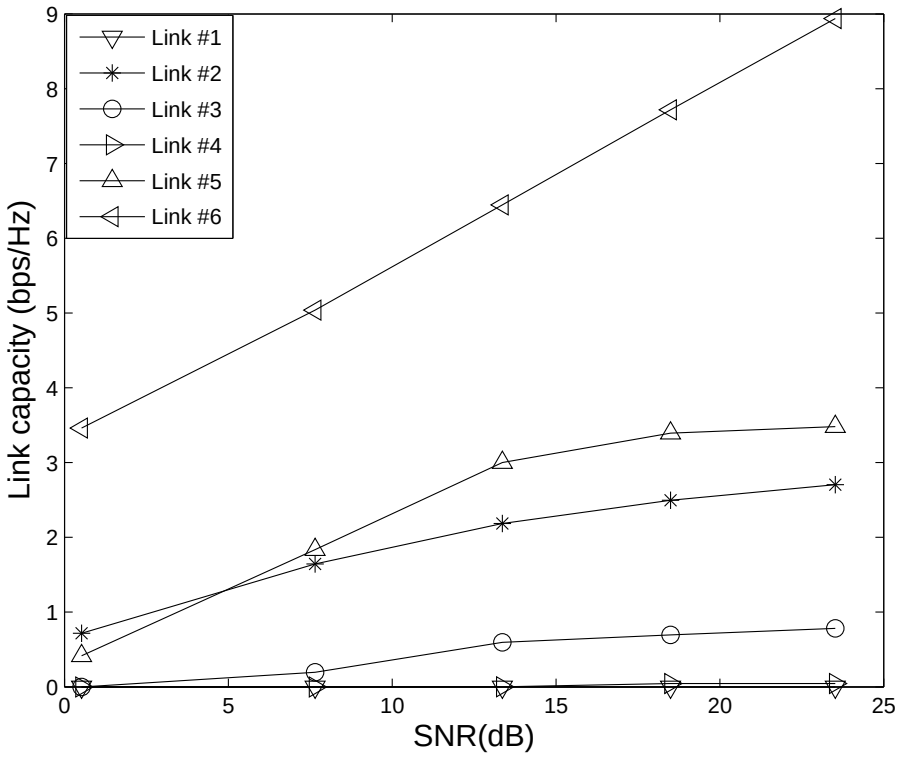

Figure 3.5: Measured link capacity versus SNR with GT power allocation in the scenario shown in Fig. 3.1.

with complete channel knowledge of all links, which allows for an optimal solution to be found. The GT approach utilizes penalties for using too much power over weak channels, thus the capacity results are greater than the MUWF scheme.

The measurement results are fairly similar to the simulations for all of the power allocation schemes. Differences between measurements and simulations can be attributed to the fact that the simulations can not possibly reproduce all of the channel effects in a real environment, notably scattering. Also, the measurement locations may not be precisely in the same location as in the simulation environment. The differences are further explored in Sec. 3.4.4.

Further, we show the CDF of the energy efficiency, Fig. 3.7 for simulated and measured scenarios. These results show that for all scenarios, the GT method is

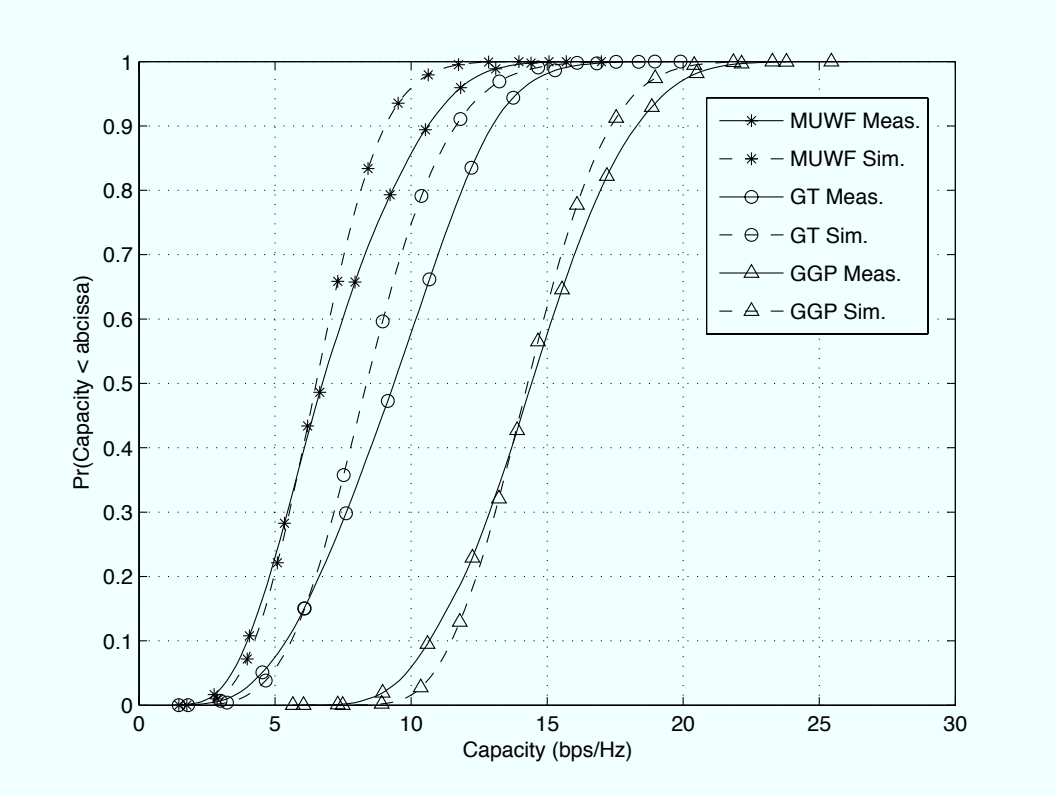

Figure 3.6: CDF of sum-rate capacities for different methods from measurements and simulations over all scenarios

more energy efficient than MUWF method and nearly as efficient as the GGP method. There are some cases when the GT method is actually more efficient than the GGP method. While the capacity performance of the GT method was near MUWF, the energy efficiency is closer to GGP. This is due to the soft-shutdown mechanism, which limits the transmitted power of links with little achievable capacity. As with the capacity CDF results, energy efficiency CDF results show good agreement between measurements and simulations.

3.4.3 Comparison of Measured Convergence Rates

An important part of any iterative algorithm is to understand the rate at which the algorithm converges. The convergence rates and what conditions impact them are discussed in [14]. It is known that the convergence time of the GGP method is high,

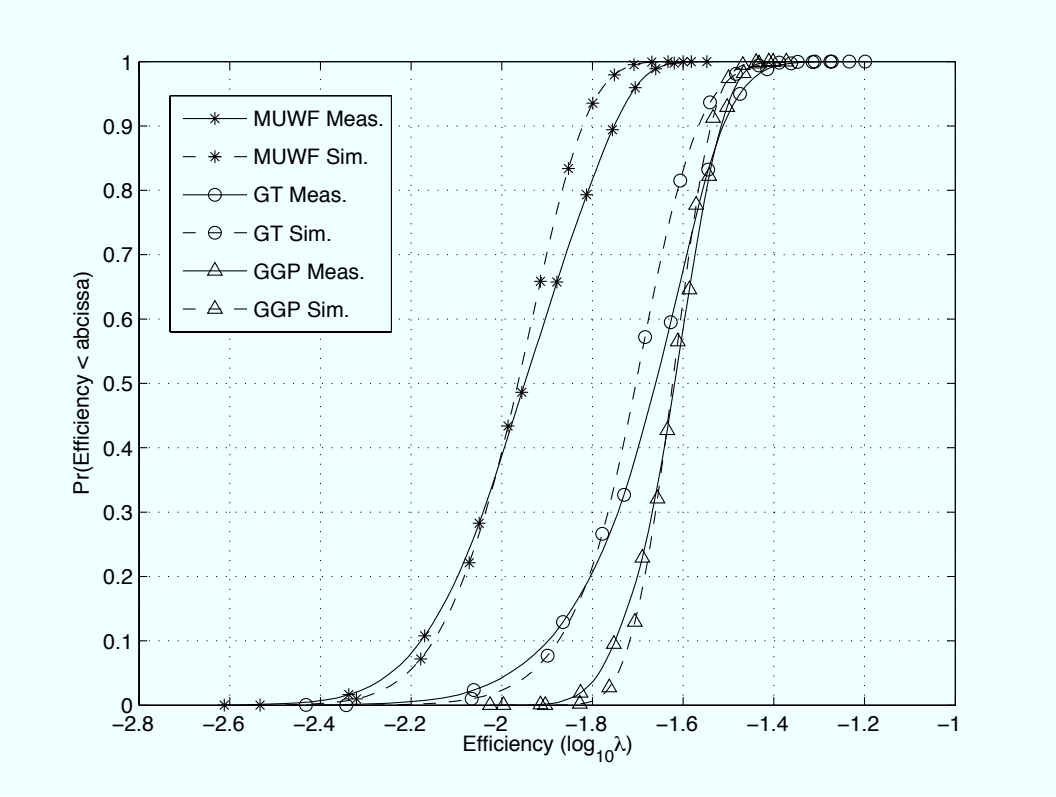

Figure 3.7: CDF of energy efficiencies for different methods from measurements and simulations over all scenarios

when compared to IWF and MUWF, due to all of the conditions in the optimization. However, the GGP method needs a centralized controller which could have very high processing power. The convergence rate and uniqueness of the equilibrium of the GT method is shown in [26]. As a point of comparison, the CDF of the convergence rates for the different methods from our scenarios is shown in Fig. 3.8. The convergence rate for MUWF and GT, shown in Fig. 3.8(a), are similar with means of 10.5 and 7.5 iterations respectively. As expected the the rate for the GGP method, shown in Fig. 3.8(b) is much higher with greater standard deviations and a mean of 186 iterations. These results illustrate that the high capacity performance of the GGP method comes with a significant price. Techniques like GT that can achieve similar performance to GGP at a fraction of the convergence time are thus desirable.

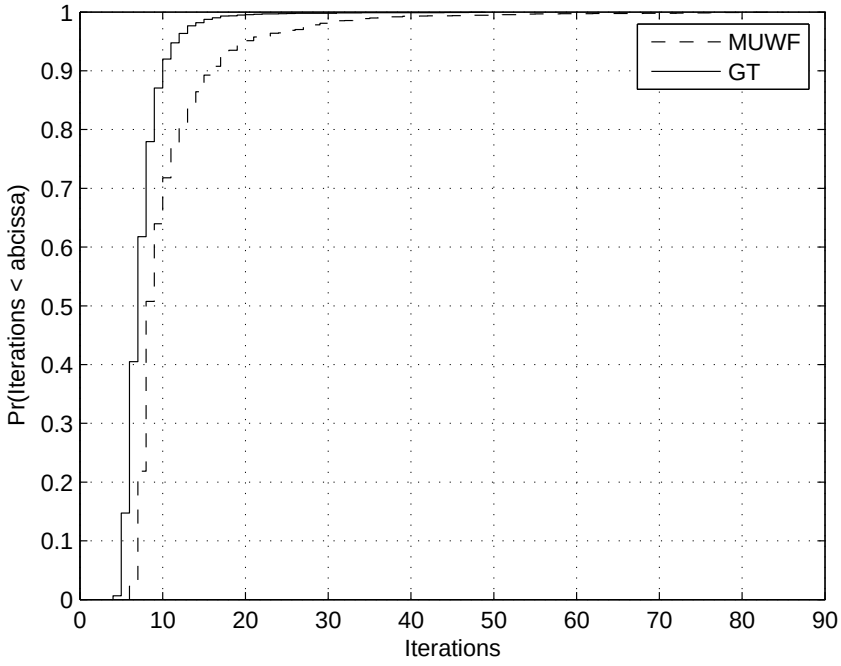

(a) MUWF and GT

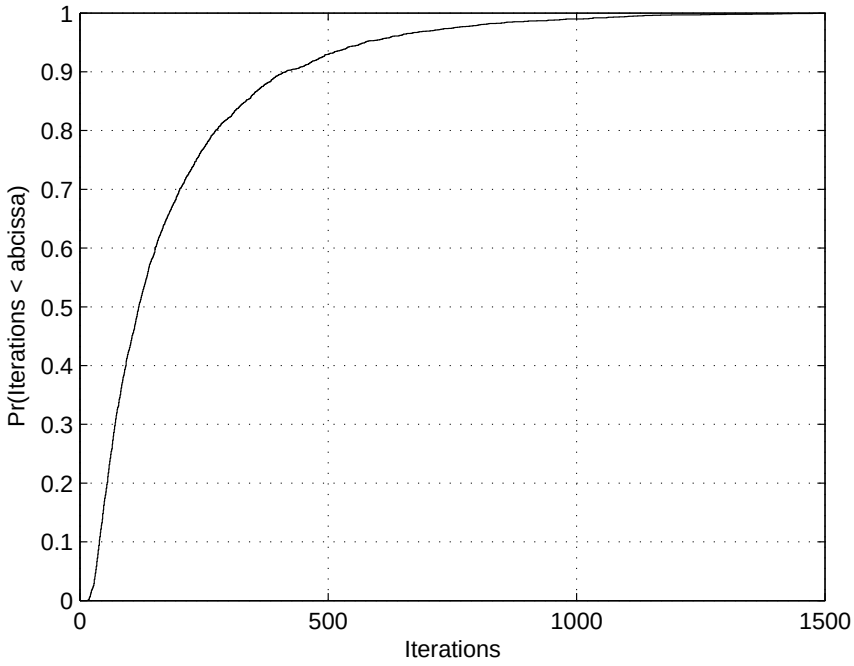

(b) GGP

Figure 3.8: CDF of the convergence rates of the power allocation methods from measurements

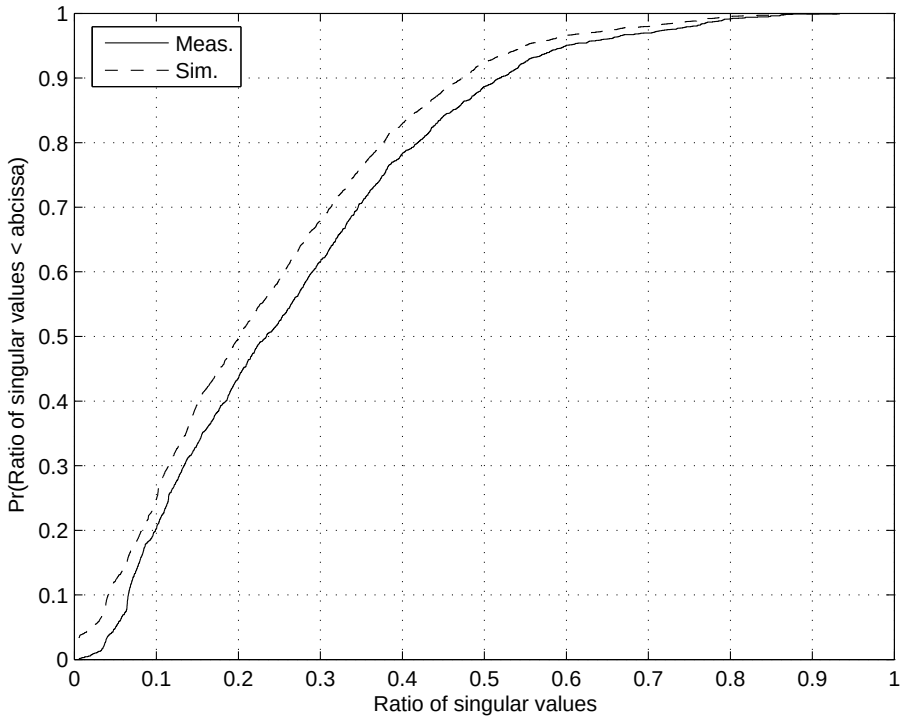

Figure 3.9: CDF of the ratio of singular values from measurements and simulations

3.4.4 Comparison of Simulation and Measurements

To provide a comparison between measured and simulated channels, Fig. 3.9 shows a CDF of the ratio of singular values (smaller singular value over larger singular value) for measured and simulated channels. Figure 3.9 shows the distribution of the singular value ratios for the 3,600 (i.e., 6 transmit positions x 6 receive positions x 100 samples) measured and simulated channels. The ratio is greater for the measured channels, which shows that the measured channels are more uncorrelated. This result makes sense because simulated channels are an approximation of the actual environment and do not include all possible features in the multipath environment. These additional multipath features have been shown to decrease channel correlation and increase singular value ratios [27]. It is important to note that the distributions are very similar except that the measured channels are shifted to higher ratios.

3.5 Conclusion

In this chapter, experimental and simulated results for different power allocation methods in an indoor MIMO local area network have been shown. Measured link capacity for one scenario was presented to show how each power allocation method performs differently. The performance of the GT method was compared to MUWF and GGP methods in terms of capacity and energy efficiency. Additionally, the probabilistic results show that the GT method outperforms the MUWF approach and approaches the performance of the GGP method (without as much network overhead). These results quantify the benefits, in terms of capacity and energy efficiency, of using greater levels of network knowledge in MIMO ad-hoc network power allocation.

Chapter 4. Antenna Spacing

4.1 Introduction

Multiple Input Multiple Output (MIMO) techniques offer great potential to enhance future wireless local area networks (WLANs) and ad hoc networks. MIMO systems can provide reliable communication by exploiting multiple spatial paths in a complex propagation environment and can also offer high capacity by creating multiple data pipes in space. This technology is ideally suited for next-generation multi-hop networks [28, 29].

As the application of MIMO technology in ad hoc networks grows, MIMO interference avoidance and compensation algorithms are of greater importance. [15, 24] studied the interactions and capacity dependencies of power allocation methods in MIMO interference systems and [14, 30–32] explored methods for power management and interference avoidance in MIMO systems.

The MIMO communications channel is affected by channel and array properties [10]. Antenna correlation contributes to the efficacy of a communication channel. Antenna correlation is a result of their physical separation and the effect of the mutual coupling on a nearby scattering body [27, 33–37]. A general background on spatial correlation and its impacts are highlighted in [27]. Notably the authors showed how mutual coupling affects the correlation of the channel and how the angular distribution of received energy affects the capacity. Results with semi-correlated channels were presented in [36], which actually show that higher antenna correlation can lead to higher capacity. This result occurs when using beamforming with a large number of users, which they have shown in simulation.

The analytical work by Tulino et. al. [33], analyzes the effects of antenna correla-

tion on capacity while considering the tradeoffs of power and bandwidth. Specifically, they show that higher correlation between antennas at the receiver reduces capacity, but not received power. Further, higher correlation at the transmitter reduces the effective dimensionality of the channel; however, power can be focused using beamforming techniques.

It is well known that, in a single link, an increase in antenna spacing results in less correlation and therefore, higher capacity. The experimental work in [38] shows that greater antenna spacing increases the capacity. However, in an ad hoc wireless MIMO network, increasing the antenna spacing also increases the spacing in the arrays of the interferers which de-correlates the interfering channels. Further, the more interferers there are, the more uncorrelated the sum interference channel becomes. Quantifying the impact of antenna spacing in MIMO ad hoc networks is the motivation for our work.

In our analysis, we specifically look at an interference limited ad hoc communication systems. The capacity is no longer just a function of a single link of interest, but rather of all the interfering transmissions. Webb et. al. [17], showed that MIMO communications are limited by a high number of interferers. Their work considers a lower bound on capacity using the law of large numbers for an increasing number of interfering antennas and nodes.

The aforementioned studies show that in interference-free communications, greater antenna spacing, due to low antenna correlation, leads to high capacity (lower BER). Further, with an increase in the number of interferers in MIMO ad hoc networks, the gain from the modes/streams/degrees-of-freedom is reduced. We will consider what happens in a MIMO ad hoc network when the antenna spacing in all nodes increases. Capacity should increase; however, the spacing in the array of the interferers also increases (assuming uniform node design). In this chapter, we will also quantify how i.) interfering node power, or the interference-to-noise ratio (INR), ii.) number of

interferers, and iii.) the power of the link of interest, or signal-to-interference ratio (SIR), impact link and network capacity.

The contribution of this chapter is to use our MIMO testbed, along with analytical channel models, to characterize the MIMO communication channel and interference environment present in a practical ad hoc network. In particular, we consider different antenna spacings and scenario sizes in an indoor ad hoc network to evaluate the effect of variable array element spacing.

In an effort to explain these findings, MIMO ad hoc network channels were analyzed using both the sum and ratio of the singular values of the wireless communication channel. An intuitive description of the inter-play between these two metrics are given. Another contribution of this work is an analysis of the different antenna spacings in an environment with certain conditions. Through this understanding of the impact of spacing on the channel singular values, a network designer would be able to create design guidelines for MIMO antenna systems in ad hoc networks devices to increase capacity. This dissertation includes indoor experimental results and supporting simulations using ray-tracing software [21, 22].

This chapter is organized as follows: Section 4.2 presents the channel and interference model of MIMO ad hoc networks, the simulated channel model, and the analytical tools to evaluate network channels. Section 4.3 provides an analysis of the singular values of a wireless channel to explain the inter-relation of the sum and ratio of singular values in a co-channel interference (CCI) limited MIMO system. Section 2.3 describes the experimental testbed that was used to collect channel and interference data in an indoor environment and the test parameters. Section 4.4 presents measurement and simulation results. Section 4.5 concludes the chapter and makes suggestions for further research.

4.2 Network and Channel Models

In this section, details on channel model are provided along with an explanation on capacity in a co-channel interference limited network.

4.2.1 Channel and Interference Model

Consider an ad hoc network (2.2) with a set of links denoted by $\mathcal{L} = \{1, 2, ..., L\}$, where each link undergoes co-channel interference from the other $L-1$ links. Each link uses N_t transmit antennas and N_r receive antennas. The matrix channel between the receive antennas of link l and the transmit antennas of link j is denoted by $\mathbf{H}_{l,j} \in C^{N_r \times N_t}$. Our analysis and measurements focus on a 2×2 scheme due to our experimental testbed. We can acquire $\mathbf{H}_{l,j}$ through channel training in the MIMO-OFDM ad hoc network testbed (described in Section 2.3) or by a synthetic channel model realized by indoor ray-tracing simulations (see Sec. 2.5).

The single channel model (2.4) used is the same in Ch. 2. In this chapter we focus on equal power allocation $\left(\mathbf{Q}_l = \mathbf{I}\frac{P_l}{N_t}\right)$ in order to analyze closed form results of the expected channel capacity. In equal power allocation for a given total power that can be transmitted by each node, P_l, the power is allocated equally to each antenna. Similarly, each link l, will receive co-channel interference from the other $L-1$ links. This interference is captured in the interference-plus-noise covariance matrix, $\mathbf{R}_l$, is the same as (2.5)

4.2.2 Capacity in Co-channel Interference Limited Networks

The efficacy of wireless networks using multiple antenna systems and that are limited by co-channel interference is affected by several factors: the number of users, antenna spacing, INR, and SIR. To understand how each of these factors affects communications, we will analyze the singular values of the wireless channel.

It is of interest to consider expectation of the link of interest $\mathbf{H}_{l,l}$ separately from the $E\{\mathbf{R}_l\}$. However, there is little we can say about the singular values of the expectation of the interference-plus-noise covariance matrix, although empirical distributions could be used. As previously published in [17], the more correlated the matrix, the less "spread out", or close to white, the singular values will be. However, this correlation does not affect the sum of the singular values of the covariance matrix and does not provide a complete explanation of the dynamics of element spacing, SIR, and INR.

These channels, notably, have some amount of correlation. Therefore, a method to analytically show how the antenna correlation (spacing and number of interfering links) impacts the capacity is need. Considering (2.4), since $E\{\log_2(f(x))\} \leq \log_2(E\{f(x)\})$, the expectation can be moved inside the logarithmic function. Therefore, the "whitened" channel $\mathbf{H}_w = \mathbf{R}_l^{-1/2}\mathbf{H}_{l,l}$ can be considered. This whitened channel includes the effects of the correlation between antennas at the transmitter and the receiver for the link of interest and all of the interfering links.

To analyze the network scenario under certain conditions, e.g. a certain antenna spacing and number receivers, the capacity for the whitened channel can be used in (2.4). The upper-bound on capacity is then

$$E\{C\} \leq \log_2\left(\det\left(\mathbf{I} + \frac{\mathrm{SNR}}{2}E\{\mathbf{H}_w\mathbf{H}_w^{\dagger}\}\right)\right), \tag{4.1}$$

where SNR is the signal-to-noise ratio. This is a closed form solution however, it is well known that this upper bound is not very tight. The problem here is two fold. There are several important results for capacity networks where a large number of degrees of freedom (antennas) [11,39]. However, in a practical system there is a limit to the number of antennas that can be deployed. In this case, there are only two antennas. Therefore, not much can be said about the distribution of the channel

matrices, thus it is difficult to find an upper bound.

There has been some work on the distribution of when the number of elements is small [40, 41]; little published research has considered the co-channel interference. There is published research that solves the capacity problem in a co-channel limited environment with antenna correlation [42, 43]. In [42], the problem is simplified by only consider antenna correlation at the transmitter. More recently, the reformulation linearization technique is employed in [43], which adequately finds the upper bound of the capacity with co-channel interference and antenna correlation. However, it is difficult to make any inferences about the network conditions from the singular values. Finally, in Moustakas, et al [44], the random channel matrices are analyzed with a *replica approach* more commonly used in physics. With this formulation, the capacity of a co-channel interference limited network with a small number of antennas can be analyzed.

4.3 Singular Value Analysis

As previously stated, we wish to understand how several different factors impact the capacity of a wireless network. For this analysis, we investigate the singular values of the whitened matrix and then present methods to understand how capacity is affected by the singular values.

4.3.1 Singular Value Metrics

First, a singular value decomposition yields.

$$E\{\mathbf{H}_w\mathbf{H}_w^\dagger\} = \mathbf{U}\begin{bmatrix} s_1 & 0 \\ 0 & s_2 \end{bmatrix}\mathbf{U}^\dagger. \tag{4.2}$$

The ratio of singular values is defined as the smallest over the largest singular

value, i.e. $R = \frac{s_2}{s_1}, r \in (0, 1]$. As the singular values become closer, the ratio goes to unity.

Next, consider the ratio of the singular values and the effect on the capacity. Assume two different whitened channels, $\mathbf{H}_w^1$ and $\mathbf{H}_w^2$ (the super-script refers to the i^{th} channel), have the same sum of squared singular values S, but one of the channels has a greater ratio of the values. In this case, $\mathbf{H}_w^1 = \mathbf{U}^1 \begin{bmatrix} \sqrt{s_1^1} & 0 \\ 0 & \sqrt{s_2^1} \end{bmatrix} \mathbf{V}^{1\dagger}$ and $\mathbf{H}_w^2 = \mathbf{U}^2 \begin{bmatrix} \sqrt{s_1^2} & 0 \\ 0 & \sqrt{s_2^2} \end{bmatrix} \mathbf{V}^{1\dagger}$. The sum is the same $s_1^1 + s_2^1 = s_1^2 + s_2^2 = S$, but the ratio, $s_2^1/s_1^1 = \alpha < s_2^2/s_1^2 = \beta$ is different, where the singular value ratio for the second whitened matrix $\mathbf{H}_w^2$, is greater[1]. Therefore, the capacity for $\mathbf{H}_w^2$ is greater for all possible power levels.

Proof 1 *Given a power P, the capacity C in terms of the ratio of singular values $R = \frac{s_2}{s_1}$ for a whitened channel is $C = \log_2((1 + s_1P)(1 + s_2P)) = \log_2((1 + s_1P)(1 + Rs_1P)) = \log_2(f(r))$. Because $\log_2$ is a monotonically increasing function, it suffices to show that the function, $f(R)$ is increasing in $R \in (0, 1]$. The derivative of $f(R)$, $\frac{df(r)}{dr} = s_1P + s_1^2P^2 > 0 \; \forall R$. Therefore, singular values that are more spread out leads to a lower ratio, which yields a lower capacity.*

Third, assume two different whitened channels again; however, now let the ratio be equal and the sum be different. In this case, the channel with the greater sum has the higher capacity.

Proof 2 *Given a power P, the capacity C in terms of the sum of singular values $S = s_1 + s_2$ for a whitened channel is $C = \log_2((1+s_1P)(1+s_2P)) = \log_2((1+s_1P)(1+$*

---

[1]The sub-script of singular values indexes the singular value for one matrix and the super-script indexes the matrix.

$(S - s_1)P)) = \log_2(f(S))$. *Because* $\log_2$ *is a monotonically increasing function, it suffices to show that the function,* $f(S)$ *is increasing in* S. *The derivative of* $f(S)$, $\frac{df(S)}{dS} = P + s_1P^2 > 0 \ \forall S$. *Therefore the channel with the greater sum of singular values yields a higher capacity.*

This decomposition shows there is a contradiction when designing the spacing between array elements using the ratio and sum of singular values. The larger the spacing the greater the capacity due to the richness in the multi-path environment [37]. However, greater spacing also leads to a smaller sum of the singular values. The sum is intuitively the ratio of the channel gain to the interference. Therefore, we investigate a balance between the ratio and sum of singular values and their impact on capacity.

4.3.2 Correlation and Sum of Singular Values

The following explanation shows why smaller antenna spacing or more correlated (specifically from interfering channels) noise leads to a greater channel gain. That is to say, the sum of singular values leads to greater channel gains under certain conditions. Recalling the expected capacity from Eq. 4.1, if the link is only limited by noise, with noise covariance matrix $\mathbf{R}_l$ (or more simply $\mathbf{R}$), the singular value decomposition is $\mathbf{R} = \mathbf{U}\begin{bmatrix} n_1 & 0 \\ 0 & n_2 \end{bmatrix}\mathbf{U}^\dagger$. With more correlated the noise, the ratio of $\frac{n_2}{n_1}$ becomes lower, while $n_1 + n_2$ (the noise power) remains the same. The noise-plus-interference covariance matrix in (2.5) is inverted in (2.6) so the singular values of $\mathbf{R}^{-1}$ are $1/n_1$ and $1/n_2$.

Now consider the link of interest channel matrix, $\mathbf{H}_{l,l}$. We take the decomposition, $\mathbf{K} = E\{\mathbf{H}\mathbf{H}^\dagger\} = \mathbf{V}\begin{bmatrix} c_1 & 0 \\ 0 & c_2 \end{bmatrix}\mathbf{V}^\dagger$ and let $\mathbf{X} = E\{\mathbf{H}\mathbf{H}^\dagger\}\mathbf{R}^{-1} = \mathbf{K}\mathbf{R}^{-1}$. Because $\mathbf{K}\mathbf{R}^{-1}$ is not Hermitian, the singular values do not coincide with the eigenvalues.

However, from Theorem 3.3.13 a) in [45], we see that the sum of ordered eigenvalues is upper-bounded by the sum of the ordered singular values.

Using the fact that the trace of a matrix is equal to the sum of its eigenvalues, the sum of the eigenvalues of $\mathbf{X}$ can be evaluated. Theorem 3.3.14 a) in [45] states that the sum of the ordered singular values of the product of two matrices is upper-bounded by the sum of the product of the ordered singular values of each of those matrices. Let $\sigma_i(\mathbf{T})$ be the i^{th} ordered singular value of matrix $\mathbf{T}$. By applying this theorem we have,

$$\text{Tr}\{\mathbf{X}\} = \sum_{i=1}^{2} \lambda_i(\mathbf{K}\mathbf{R}^{-1}) \leq \sum_{i=1}^{2} \sigma_i(\mathbf{K})\sigma_i(\mathbf{R}^{-1}) = \frac{c_1}{n_2} + \frac{c_2}{n_1} \tag{4.3}$$

It is now straight froward to show that as $n_2/n_1 \rightarrow 0$ (i.e., as the correlation of the noise increases) the upper bound of $\text{Tr}(\mathbf{X})$ gets bigger. Notice that the sum does not depend on the channel correlation (i.e., the ratio of c_2/c_1), only on the noise correlation. Finally, the number of interferers and the antenna spacing influence the noise correlation. For larger antenna spacings and more interferers, there is a lower sum of squared singular values.

4.3.3 Balance between Sum and Ratio of Squared Singular Values

In our experiments, the capacity in a co-channel interference system is more complicated because the ratio and the sums of squared singular values are both variable, depending on the array element spacing and the channel. In this section, we develop "crossing points" or decision making thresholds to decide what size antenna spacings are more desirable to maximize capacity in a MIMO network with co-channel interference. Given two whitened channels, the first channel has sum $S^1 = s_1^1 + s_2^1$ and ratio $R^1 = \frac{s_2^1}{s_2^1}$ and channel two has $S^2 = s_1^2 + s_2^2$ and $R^2 = \frac{s_2^2}{s_1^2}$, where $S^2 > S^1$ and $R^2 < R^1$.

Proposition 1 *For channel 1 to have greater capacity than channel 2, the power needs to be greater than zero therefore,* $(S^1)^2R^1(R^2+1)^2 - (S^2)^2R^2(r^1+1)^2 > 0$.

If this condition is met, channel 1 will have greater capacity than channel 2 for power levels greater than $\frac{(S^2-S^1)(R^2+1)^2(R^1+1)^2}{(S^1)^2R^1(R^2+1)^2-(S^2)^2R^2(R^1+1)^2}$. *Otherwise, channel 2 will have greater capacity because the channel gain will be higher due to the larger sum of squared singular values.*

4.4 Results

In this section, analysis of the sum and ratio of singular values from the simulations and measurements of the network scenarios are given. The environment and description of measuring the different scenarios is described in Sec. 2.4. It should be noted, in the case of 3λ antenna spacing with the simulated channels, that the ratio of singular values grows with an increasing number of interferers more quickly than in the measured channels. This general trend can be attributed to the simulated channels having less correlation than the measured channels. Normalization is performed on the channels (Sec. 2.2), however the same normalization factor can not be performed for both the simulations and the measurements. This leads to an offset in the capacity seen in some of the results.

The different antenna arrays used in our field experiments and simulations were omni-directional antennas. We chose to evaluate antenna spacings, d of $\lambda/2$ and 3λ, where λ is the wavelength in free space. We selected these contrasting distances because $\lambda/2$ is a commonly chosen separation and 3λ is large, but manageable in an indoor wireless network.

The channels measurements and simulations were made with the details in Ch. 2. The total power available for each link was initialized to 100 times above the noise floor. For each scenario, the expected capacity was calculated for the average of all

100 snapshots.

4.4.1 Evaluation of Singular Values

In our findings, array element spacing changes the correlation of both the channel of interest and the interference channels. From the ratio and the sum of the squared singular values of the covariance of the whitened channel matrix, we observe that:

1. Greater array element spacing leads to a greater ratio of singular values

2. Greater array element spacing leads to a smaller sum of singular values

These observations are presented in the following sections and can be seen in Figs. 4.1 and 4.2.

4.4.1.1 Ratio of squared singular values

To demonstrate the first observation, we consider the ratio of singular values from Sec. 4.3.1. The simulated and measured ratio of the squared singular values of the whitened channel matrix, for both antenna spacings and various scenario sizes, are provided in Fig. 4.1. For both low (Fig. 4.1(a)) and high (Fig. 4.1(b)) INR, greater spacing has a higher ratio. This shows that the channels with greater antenna spacing are becoming more uncorrelated. Intuitively, this result shows that greater antenna spacing decreases the value of the difference between the singular values. As the number of interferers increases, the ratio also increases. In our measurements, the rate of growth with the addition of interferers is similar for both antenna spacings. Further, the evolution of the ratio of singular values with increasing interferers is similar for measured and simulated channels. Alone, these results are simular to [17]. However, the sum of singular values presents greater information to the antenna spacing and scenario size problem.

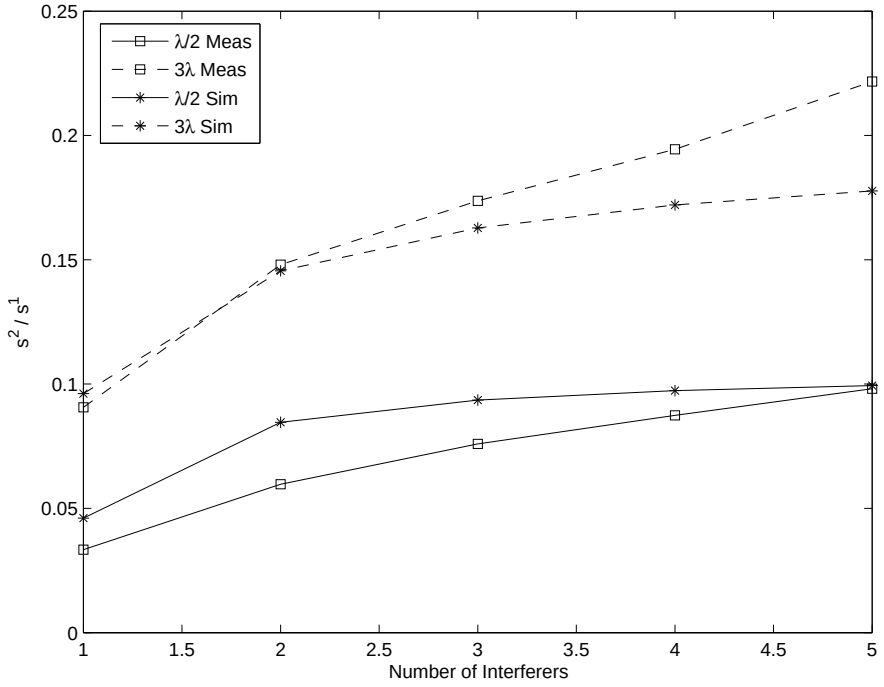

(a) INR = 10 dB

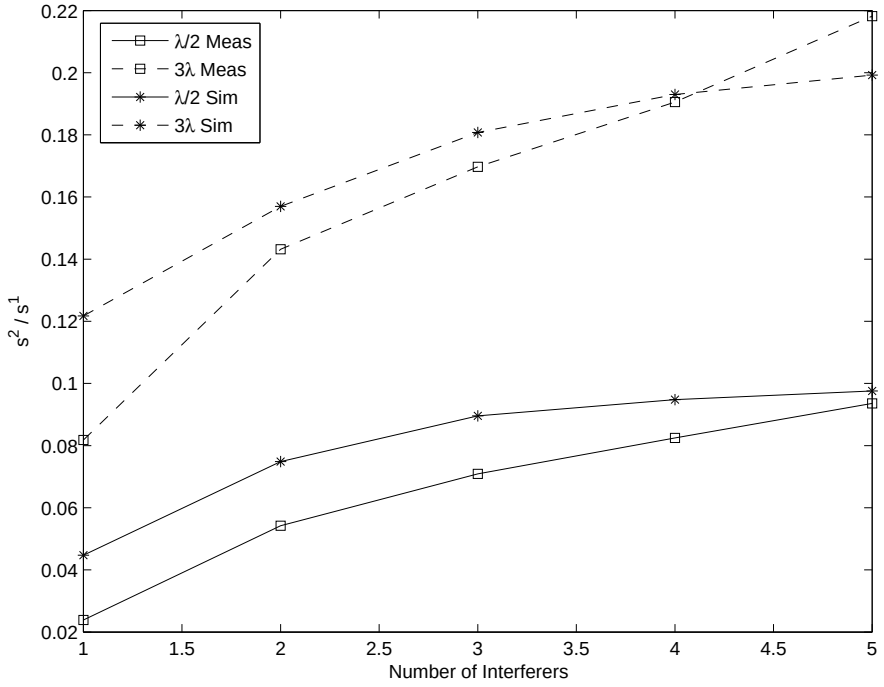

(b) INR = 20 dB

Figure 4.1: Ratio of squared singular values vs. number of interferers

4.4.1.2 Sum of Squared Singular Values

The second observation is shown with simulated and measured results for the sum of squared singular values for both antenna spacings versus the number of interfering links in Fig. 4.2. First, as the number of interferers increases, this sum decreases. Second, the smaller antenna spacing ($\lambda/2$) has a higher sum, which leads to a larger channel gain. This is demonstrates that while larger antenna spacings can be beneficial for a single MIMO link [37], they are not always beneficial in interference limited MIMO networks where all interferers have the same spacing. The importance lies in the fact that MIMO networks can have greater capacity with closer spaced antennas depending on the number of interfering nodes.

Another interesting observation is that sum of squared singular values for both antenna spacings decrease with increasing INR, for the measured channels and simulated channels. An increase in INR, as seen in the comparison of Fig. 4.2(a) to Fig. 4.2(b), results in a lower sum of singular values. This interplay between the ratio and sum of squared singular values has a unique affect on the expected capacity.

4.4.1.3 Expected Capacity

It is most interesting to consider how the ratio and sum of squared singular values impact the capacity. The measured and simulated expected sum-rate capacity results for an INR of 10 dB are shown in Fig. 4.3. As expected, the expected sum capacity (bps/Hz) decreases as the number of interferers increases in all cases. Under conditions of low INR and low SIR, our measured results show a crossing point between two and three interfering links for the expected capacity with antenna spacing of 3λ working better in the presence of a greater number of interferers. However, with a higher SIR value of 20 dB, the capacity is always better for a greater antenna spacing.

When considering the simulation results, the capacity is higher for both low Fig.

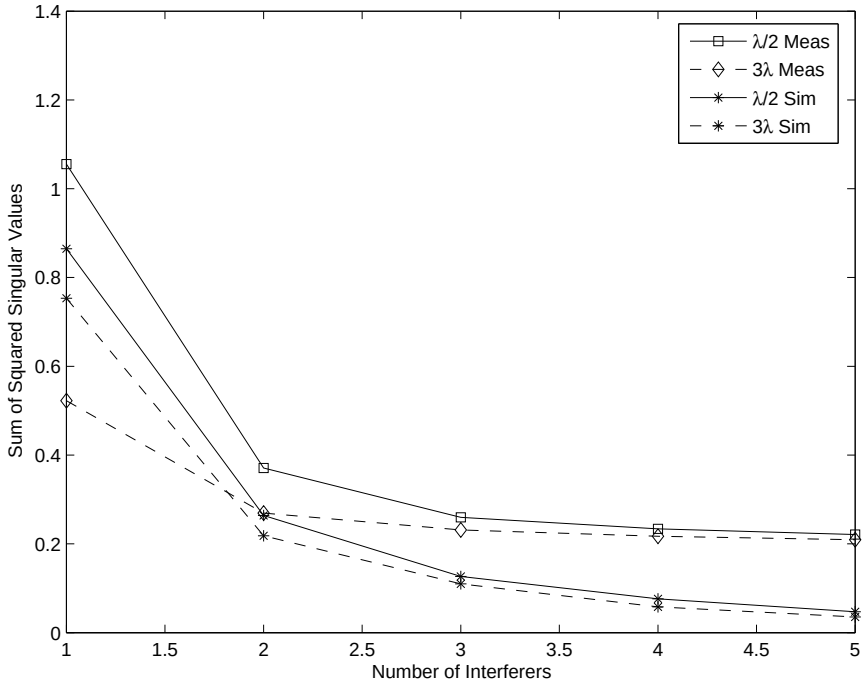

(a) INR = 10 dB

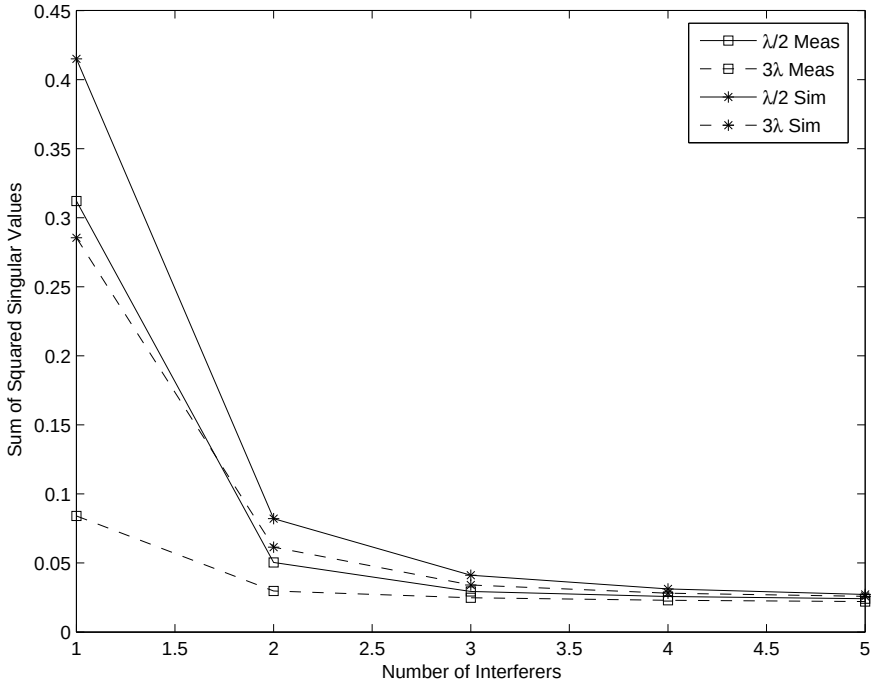

(b) INR = 20 dB

Figure 4.2: Sum of squared singular values vs. number of interferers

4.3(a) and high Fig. 4.3(b) SIR. This is a result of the aforementioned disparity between the rank of measured and simulated measured channels. More importantly, the crossing points are different. This is not surprising because while the general trends of the ratio and sums of squared singular values are the same, the slopes are not identical. So, the simulations can verify the general trends, which approximates the expected performance of the system.

Comparatively, when the interference power is increased to 20 dB (as shown in Fig. 4.4), the closer antenna spacing performs slightly better due to receiving less of the interference power with respect to the larger spacing. In Fig. 4.4(a), the smaller spacing performs better until there are three interfering links. With greater than three interferers, the gain of having a wide spacing is better. At a higher signal power (and higher interference power) in Fig. 4.4(b), the $\lambda/2$ spacing has a higher capacity than at low INR, for a low number of interferers. When the number of interferers is one, the two spacings have very similar expected capacity. However, as the number of interfering links increases, the capacity drops quickly for the small spacing. Thus it is again better to have a larger spacing when the signal power is high. Also, the capacity for all spacings and number of interfering links is very similar for a given SIR when comparing between the different interference power levels.

The general trend is that for low SIR and low number of interferers, it is measurably better to have a smaller antenna spacing, $\lambda/2$. When the number of interferers or the SIR is high, then a wider antenna spacing, 3λ yields a greater capacity. This result is due to the fact that the sum of squared singular values is high for $\lambda/2$ when the number of interferers is low (regardless of INR). As the number of interfering links increases, the capacity then becomes dominated by the ratio of the singular values. The crossing points analysis can then be done to take into account all of the interactions.

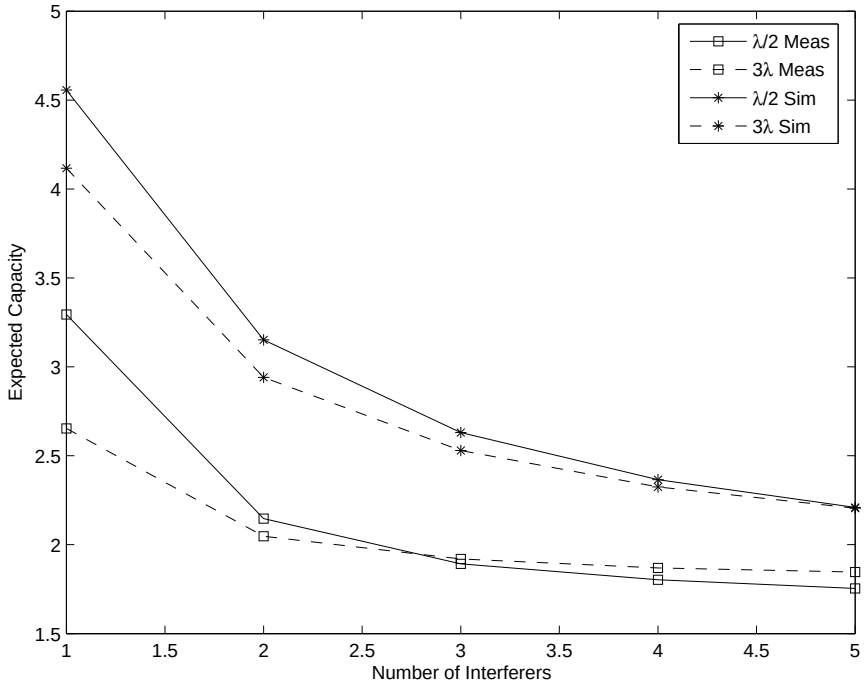

(a) SIR = 0 dB

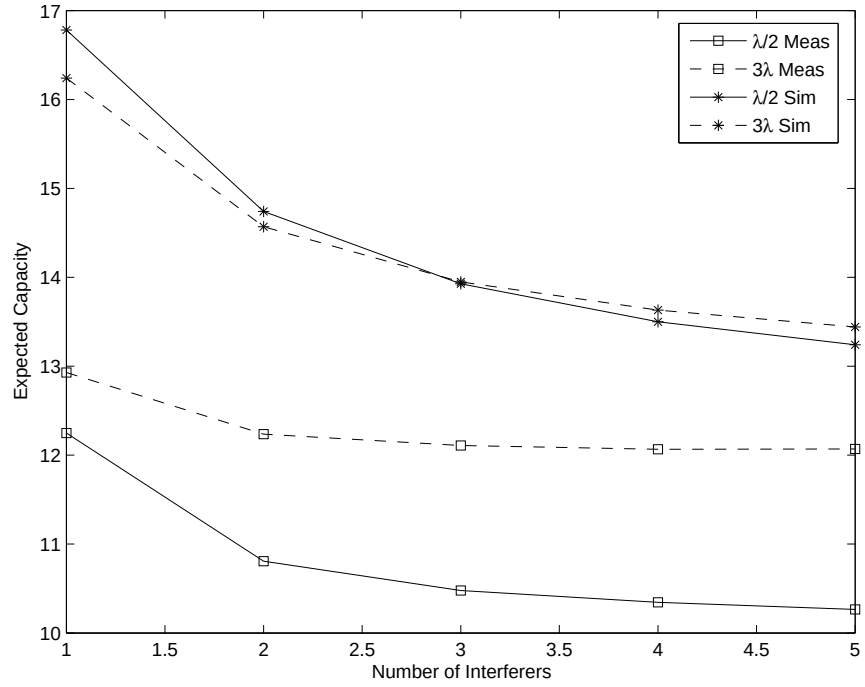

(b) SIR = 20 dB

Figure 4.3: Expected sum capacity vs. number of interferers for INR = 10 dB

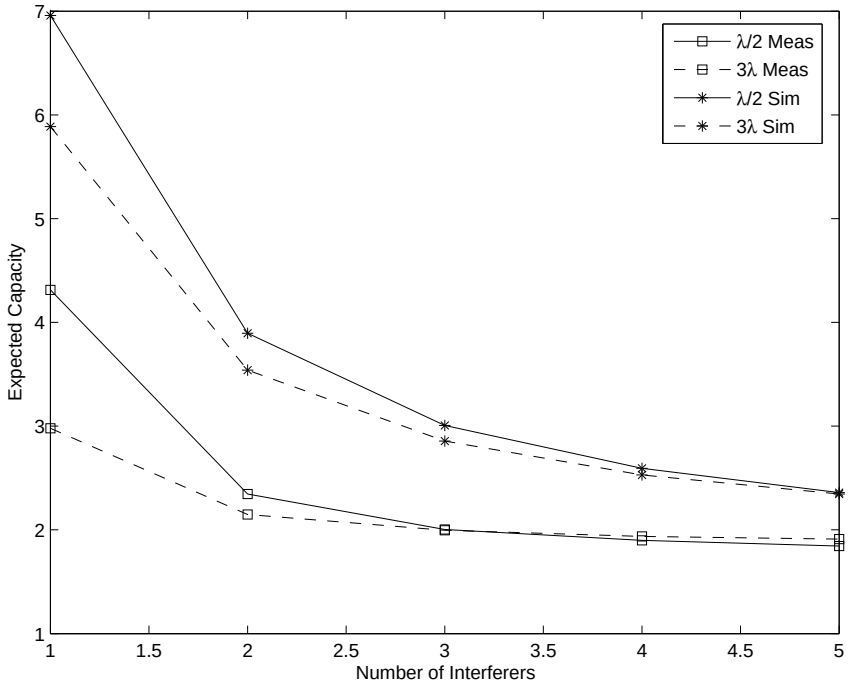

(a) SIR = 0 dB

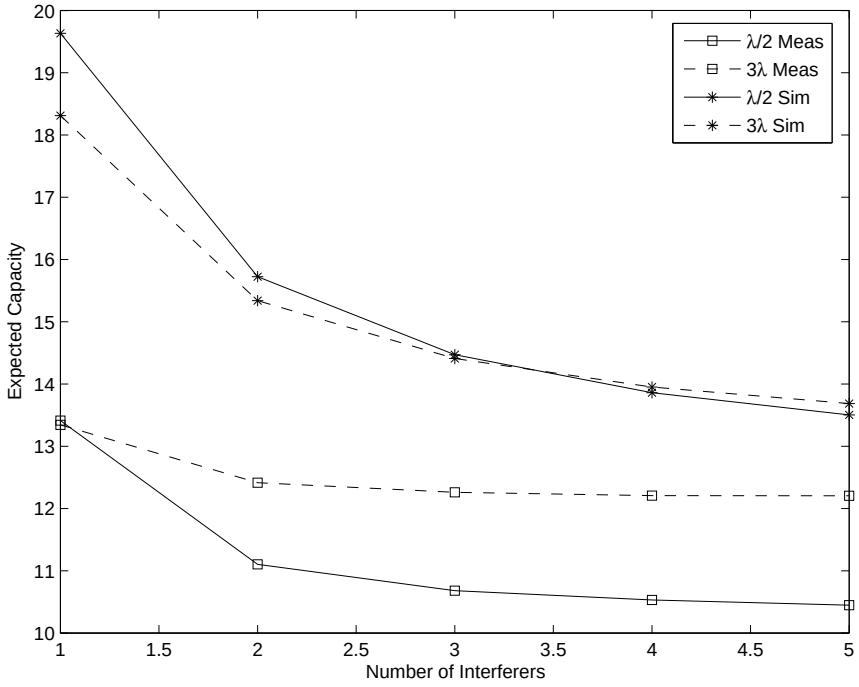

(b) SIR = 20 dB

Figure 4.4: Expected sum capacity vs. number of interferers for INR = 20 dB

4.4.2 Capacity vs. SINR

The following is an analysis of the expected capacity (bps/Hz) for different scenarios and various signal power levels, see Fig. 4.5-4.6. This analysis considers scenarios where there are one and five interferers (or two and six links in the network), to examine situations when a scenario has one and five interfering links. First, when considering 1 interfering link and there is INR, it is clear from the simulations Fig. 4.5(a) and measurements Fig. 4.5(b) that $\lambda/2$ offers the highest capacity except when the SIR is very high. When INR is high, the shorter antenna spacing outperforms the 3λ spacing. Intuitively, when there is a small number of interferers, even with moderate interference power, a small antenna spacing is more resilient to these effects and therefore has a greater capacity. This result follows from the previous explanation that the sum of singular values dominates. However, with few interferers and a larger antenna spacing, some additional capacity gain can be achieved when there is lower interference power and high signal power.

In contrast, when the number of interferers is high (Fig. 4.6) the capacity is greater for 3λ for almost all SIR. The only time $\lambda/2$ is greater is at very low SIR (≤ 0 dB) and even then the difference is marginal. This result confirms that when there are a higher number of interferers, the impact of the un-correlated interference channels (ratio of singular values) dominates the capacity. Further, when the INR power is greater, there is little impact of the capacity. Additionally, the results from the ray-tracing simulations Fig. 4.6(a) and the measurements Fig. 4.6(b) are very similar.

The capacity results are shown for our specific indoor environment. In different environments and network conditions, the gap between the capacity with 3λ and $\lambda/2$ will be different. Because both the ratio and sum of singular values increase capacity, situations that lead to a much higher value of ratio or sum, will lead to a greater gap in the capacities for the two different spacings. One such case, would be when there

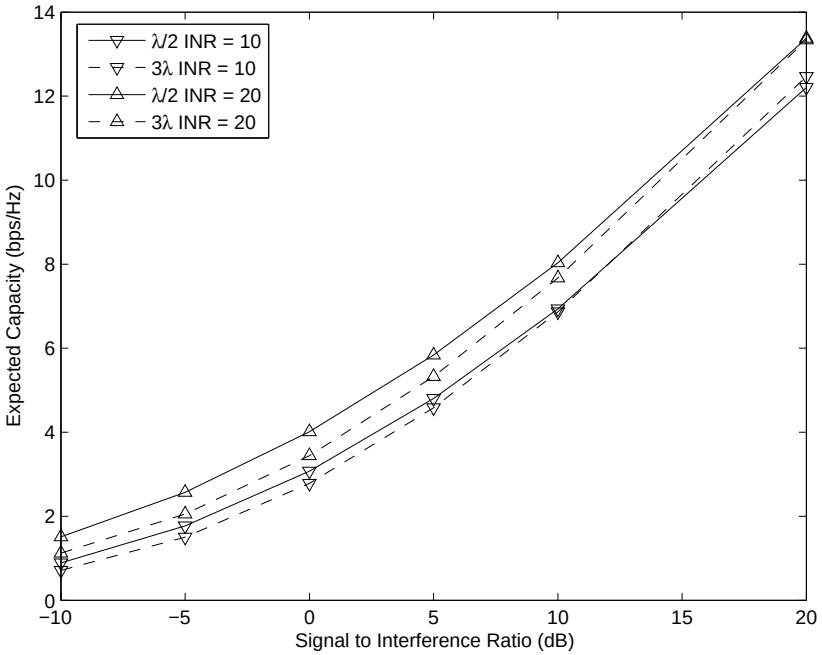

(a) Simulations

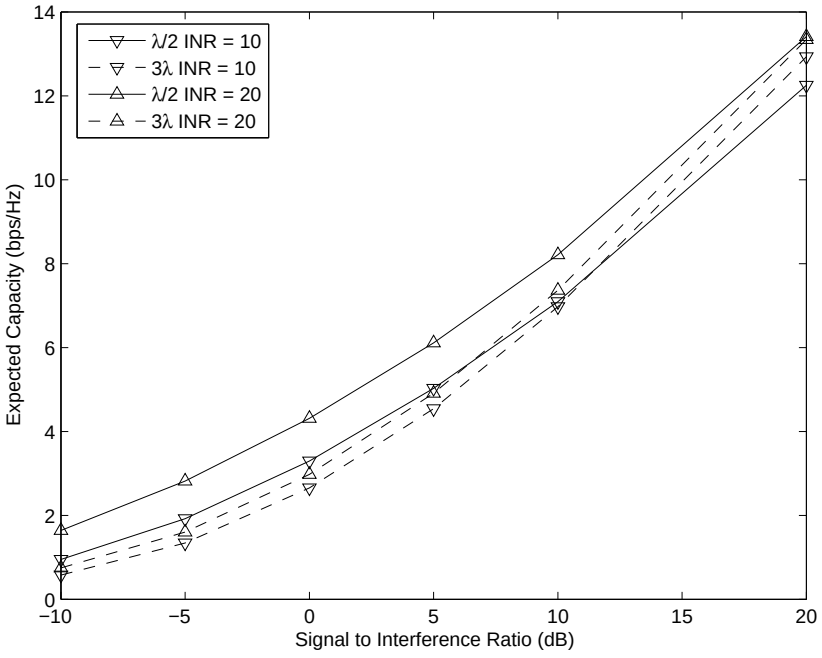

(b) Measurements

Figure 4.5: Expected capacity vs. signal to interference ratio with 1 interferer for simulated and measured channels with INR={10,20}

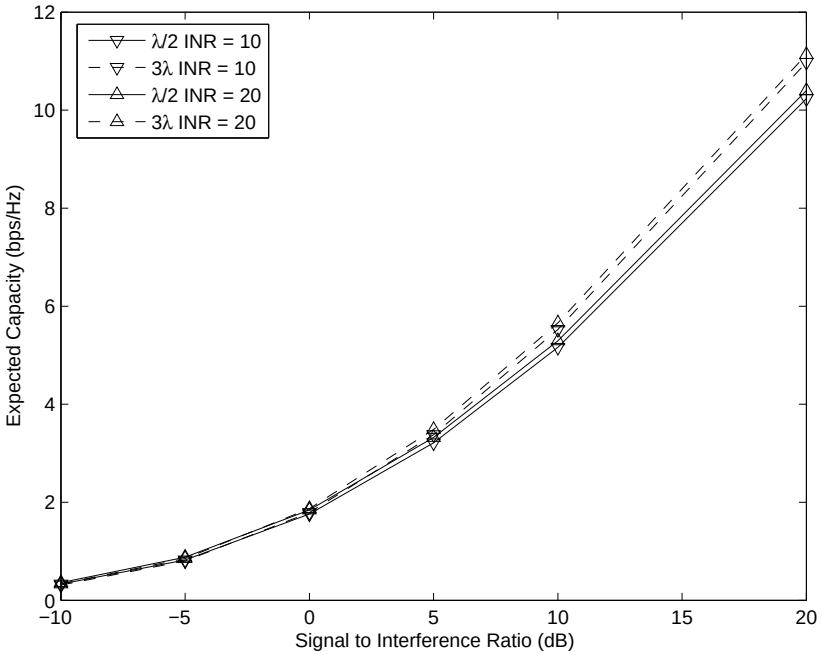

(a) Simulations

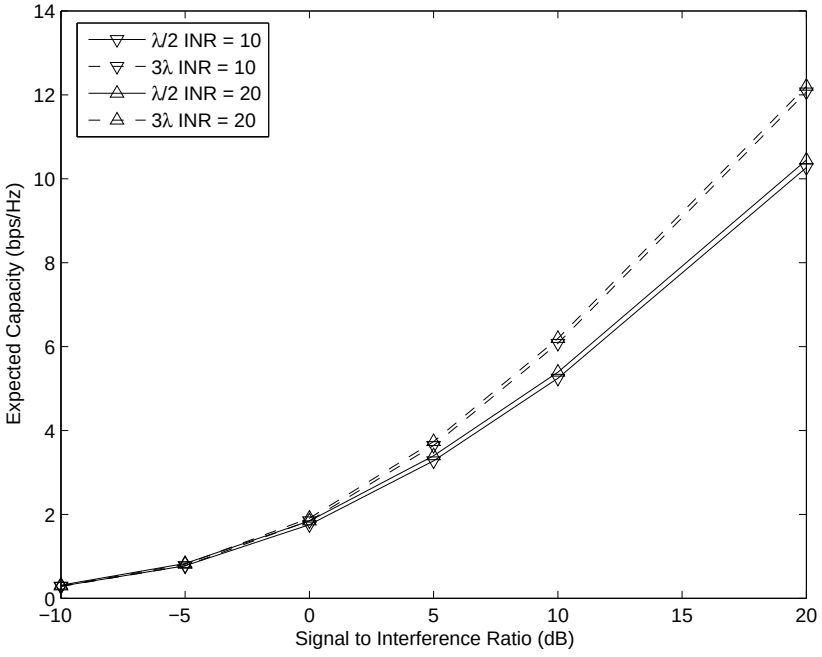

(b) Measurements

Figure 4.6: Expected capacity vs. signal to interference ratio with 5 interferers for simulated and measured channels with INR=$\{10,20\}$

is very high INR with a low number of interferers and a high amount of multipath fading. Because there is a high amount of multipath fading, there will not be much advantage to a wide spacing over a small spacing. With a low number of interferers, the noise-plus-interfererence covariance matrix $\mathbf{R}_l$ will not have a strong impact on the capacity. But with high INR, the capacity of the $\lambda/2$ spacing will receive much less interference when compared the 3λ spacing, thus the network capacities will be much different.

4.4.3 Crossing Point Level vs. SIR

Because of the interplay between the ratio and sum of squared singular values and the impact of SIR, INR, and antenna spacing, on expected capacity, we provide the crossing point results from our measured and simulated scenarios. By understanding the dynamics of this crossing point, antenna distance and network size can be tuned to meet a certain level of performance. These results are presented in Fig. 4.7 for the SIR of the crossing point (the point at which for more signal power it is beneficial to use a greater antenna spacing) vs. the number of interfering links.

The general trend is that as the number of interferers is increased, the signal power, for which higher capacity will be obtained with greater spacing, decreases. Another way of thinking of this trend is that, for low SIR, $\lambda/2$ spacing has greater capacity than 3λ spacing. The trend, of the SIR crossing point decreasing for the small versus large antenna spacings, is due to the smaller impact of the sum of singular values and the increase of the ratio of squared singular values with increasing number of interferers. When the interference-to-noise ratio is high, the SIR crossing point is also higher. Intuitively, the smaller antenna spacing yields higher capacity, in the presence of higher interference power.

As is shown, different wireless channel and environment conditions lead to dif-

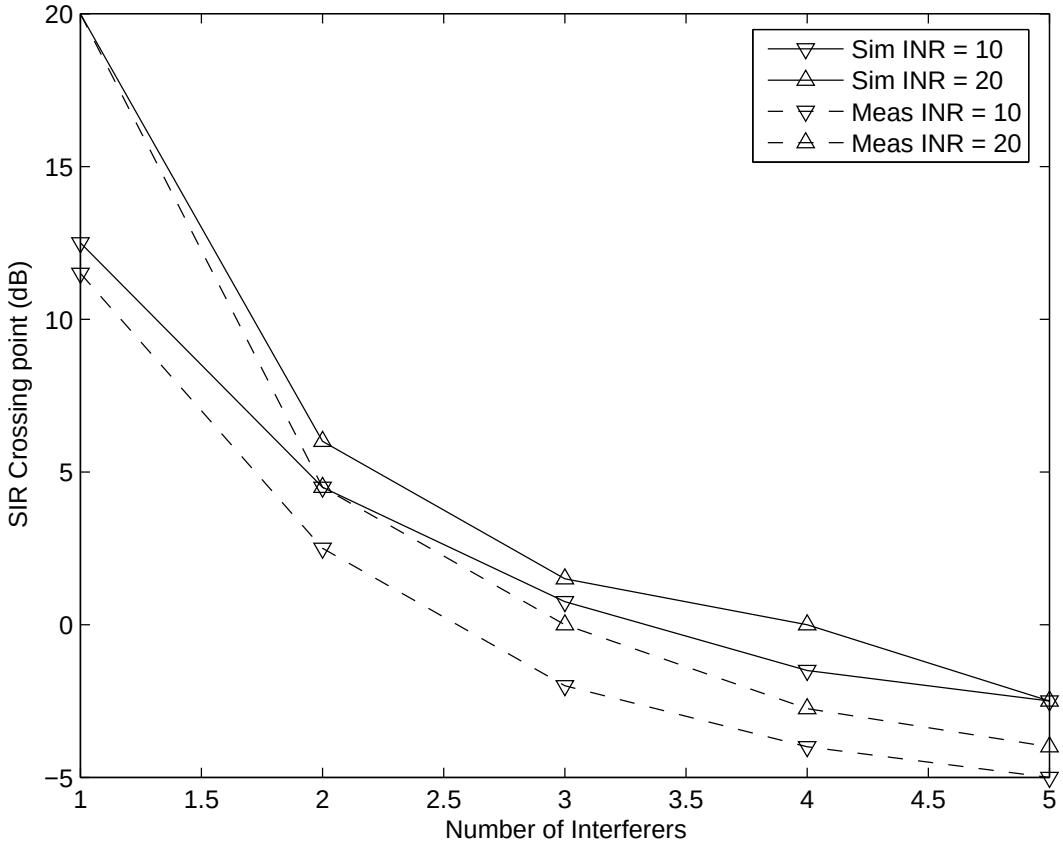

Figure 4.7: Signal to interference ratio crossing point in capacity with INR={10,20} dB for the simulated and measured channels

ferent crossing points when the capacity is higher for 3λ versus $\lambda/2$ spacing. By understanding this dynamic, a network designer can take the antenna spacing into consideration when planning a communications system of ad hoc networked MIMO nodes. Changing the spacing of the antenna array provides another method for tuning to typical operating environments and achieving higher capacity. Given the number and transmit power of co-channel interferers, one can consider other network conditions, such as the scheduling protocol and MAC functionality to estimate the SIR and INR of the system. With these values, the appropriate antenna spacing can be determined.

4.5 Conclusions

This work extends previous investigations on antenna correlation and the impact of multiple interfering links in a MIMO ad hoc network. Analytical tools were presented to understand the impact of the singular values of the channels of interest and interference. This has lead to a greater understanding of the impact of antenna spacing on the expected network capacity in an interference-limited channel of expected network capacity. A crossing point analysis was shown that allows a network designer to make a decision for best antenna spacing for a given channel environment. Capacity performance of varying numbers of interferers shows how the crossing point analysis can be used in a real network. Results presenting the power of these tools were shown with measured results and with a ray-tracing simulation.

Chapter 5. Optically Transparent Flexible MIMO Antennas

5.1 Introduction

To help wireless communication network designers utilize MIMO technology and the promised increases in capacity, standards are being adopted to facilitate the implementation of practical systems. Two new wireless communications standards 802.11n and 802.16e [46–48], both use multiple antennas to increase capacity. Given this commercial demand, the form factor of the wireless device and the incorporation of the antennas into the node is important to consider. A design challenge emerges from the form factor constraint because, in the conventional wisdom [38], increases in capacity come from spatial separation of the multiple antennas. In Ch. 4 it is shown that different antenna spacing may be more desirable under certain scenarios. However, when the size of the device inhibits various spacings, the ability to effectively integrate an antenna array system within a mobile device becomes more important.

Optical translucency allows for the potential to hide an antenna or make the antenna virtually invisible when mounted on a transparent substrate, such as the screen of a laptop or PDA. Flexibility of a material allows the antenna to be incorporated into moving structures or conform to non-flat surfaces. This chapter presents a solution to the challenge of creating antennas for small form factors by proposing antennas that are flexible, conformal, and transparent.

There is an increasing demand for transparent antennas that can be attached to non-traditional surfaces and materials, such as conformal antennas adhering to flexible fabrics and plastic substrates [49]. Antennas meeting these needs have previously been prototyped through the use of conductive inks on inflexible substrates [50–52]. These inks are conductive because they have metallic nano-particles. However, while highly

conductive, these ink antennas are not optically transparent and do not bend reliably on flexible substrates.

Indium tin oxide (ITO) became a very popular material for transparent antennas because of the high conductivity and high optical transparency [18,53]. The reported ITO antenna performs very well when compared to copper antennas; however, ITO antennas crack when flexed similar to the metallic inks.

The solution presented in this dissertation utilizes conductive polymers as a material for antennas because they can be printed to be transparent and are flexible. Conductive polymer are also desirable because of the their low cost, ease of processing, and potential for all-additive ink-jet manufacturing [8, 54, 55]. In this chapter, a conductive polymer dipole antenna array is presented in Sec. 5.2. Section 5.3 describes the fabrication process. The antenna characteristics are shown in Sec. 5.4. The flexibility and transparency of the antenna are analyzed in Sec. 5.5. Finally, the performance of the conducive polymer antenna system in a MIMO network is shown in Sec. 5.6.

5.2 Antenna Design

The design goal is to create an antenna that is flexible and transparent. These constraint limits many antenna candidates because it is desirable to have an antenna that does not require a ground plane. Antennas with ground planes, e.g. patch antennas [56], would reduce the possibility of the antenna to be transparent. With a ground plane, the fabrication process of the antenna is also more complicated because the printing would need to be done on both sides of the substrate. Therefore, an ideal candidate for a flexible and transparent antenna is one that has only co-planar elements. For simplicity, a dipole design similar to [18] was chosen.

The antenna is a center-fed dipole antenna and is designed to resonate at 2.5

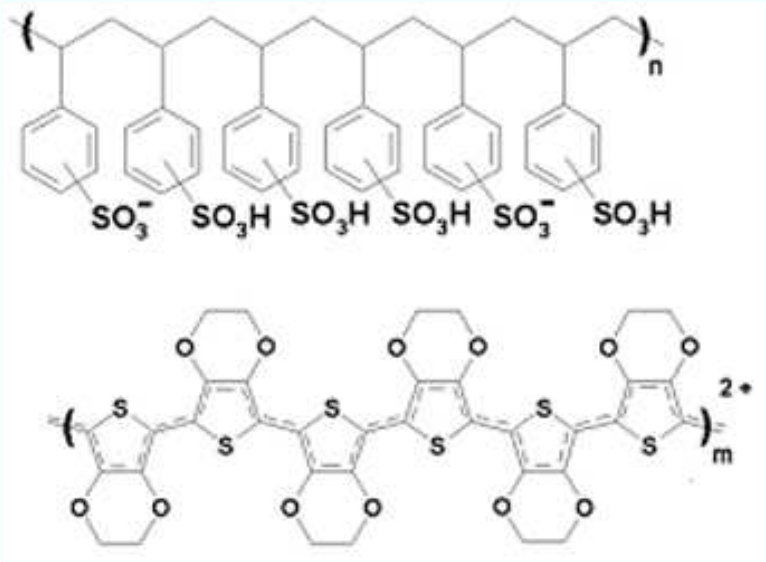

Figure 5.1: Chemical diagram of PEDOT(upper)-PSS(lower)

GHz. This traditional dipole has a total length of $\lambda/2$ or 60 mm. The arms of the dipole are 3mm wide. The fabrication technique (described in Sec. 5.3) yields a conductive polymer average thickness of approximately $25\mu m$. The antenna array will have two elements and a separation of $\lambda/4 = 30$ mm. The antenna was fabricated on a polyethylene terephthalate (PET) substrate, with a relative dielectric constant of $\epsilon_r = 3.8$ and a thickness of 0.5 mm. In addition to its translucence, this substrate was chosen for its flexibility as the resulting product could be conformable to curved surfaces.

The conductive polymer used is Clevios PH500 PEDOT-PSS, or Poly(3,4-ethylenedioxythiophene) poly(styrenesulfonate) aqueous dispersion. The chemical diagram for PEDOT-PSS is shown in Fig. 5.1. The upper compound PEDOT, has a +2 charge and the lower compound PSS, has a -2 charge. When these two compounds line up during polymerization, the form a chain with oppositely charged ends allowing carriers to flow though the chain.

By specification, this polymer has a conductivity of 300 S/m [54]. The polymer is modified with 10% Dimethyl sulfoxide (DMSO) to increase the conductivity, and

2% surfactant (Tween-21) to lower the surface tension. Through testing we have found the conductivity of our modified solution to be approximately 5×10^5 S/m, which is over two magnitudes higher than the stock PEDOT-PSS and much closer to the conductivity of copper (5.8×10^7 S/m). The polymer solution was also modified to control the thickness and consequently the transparency of the antennas. The polymer is diluted with deionized (DI) water in ratios of 1:1 and 1:2, in addition to full strength. An image of a MIMO array with 1:2 dilution is shown in Fig. 5.2.

5.3 Antenna Fabrication

Fabrication utilizing additive printing methods offers a stark contrast to traditional subtractive fabrication techniques generally used in circuit board and RF production, such as milling. As an additive process, printing can achieve patterns and geometries while using a minimum of material, which poses a large economic advantage especially when printing precious metals or other high cost materials. The additive nature of the process also allows for the use of a wide array of substrates including traditional boards such as FR-4 and ceramic-based dielectric materials. The low-temperature and non-contact nature of the process also allows for the use of many non-traditional and less rigid substrates such as plastics, polymers, fabrics, paper, and more. The cross sectional thickness of printed materials can be kept to a minimum when a small profile is needed, or more layers can be added for increased thickness.

Initial efforts in fabrication of antennas utilized a modified screen printing technique. Rather than masking a screen, the pattern mask was applied directly on the substrate and the conductive ink is administered and cured. Though this process was successful in creating several prototypes, there was very little control over the thickness of printed layers. Layer uniformity was also a problem, as curing/baking of liquid inks could leave behind meniscus artifacts that change with viscosity and sur-

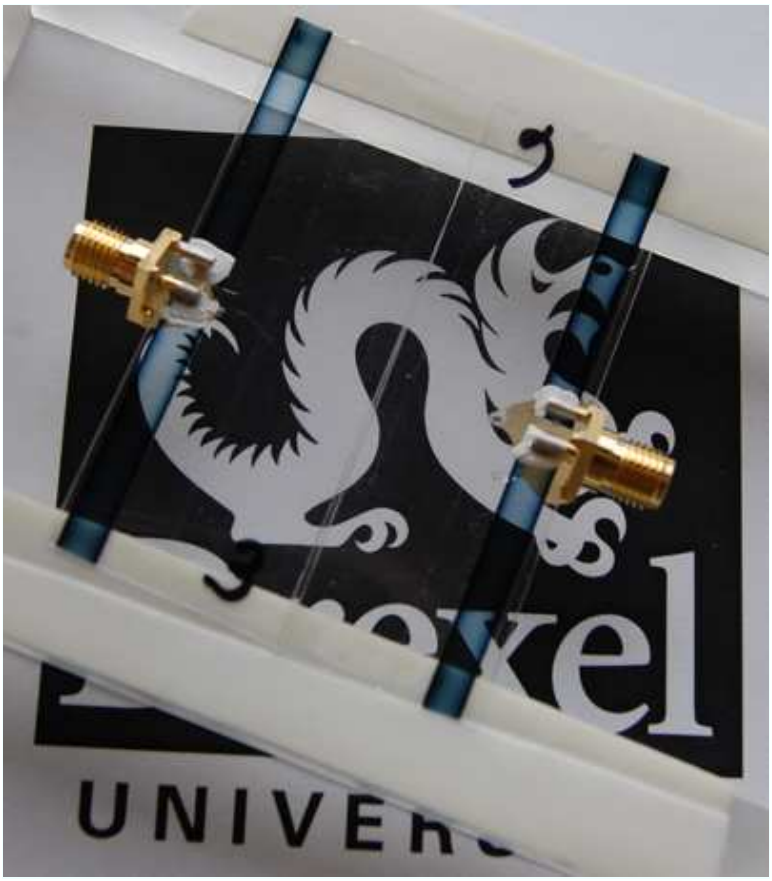

Figure 5.2: Transparent MIMO antenna array with dilution of 1:2 DI polymer to water

face tension. Therefore, future work includes creating conductive polymer antennas with a materials printer.

For comparison purposes, copper antennas were fabricated. The copper antennas were milled from one-sided copper FR-4 printed circuit board with a thickness of 2mm. Because the antennas are dipoles, the difference in dielectric constants of the substrates used (FR-4 for copper and PET for conductive polymer antennas) will not greatly affect the characteristics of the antennas.

5.4 Antenna Array Characteristics

In this section, the antenna array characteristics are analyzed. The 1:2 polymer to water dilution conductive polymer antenna array is first compared to a copper antenna array to understand how the new antennas compare to a similar, more traditional design. The antennas were measured with a network analyzer and radiation patterns were recorded in an anechoic chamber. The chamber was calibrated to a known test antenna to determine the gain in comparison to an isotropic radiator. The radiation patterns of the presented results are in dBi.

The measured return loss, or scattering parameter S_{11} is shown in Fig. 5.3. An antenna is considered "radiating" when the return loss is below -10 dB [56]. The copper antenna performs very well at the the chosen center frequency of 2.5 GHz. The return loss of the conductive polymer antenna is -12 dB at 2.5 GHz, which means that it is radiating but may not have very high gain.

The radiation patterns of the copper and the diluted conductive polymer antenna arrays measured in the anechoic chamber are shown in Fig. 5.4. The MIMO array radiation patterns are presented for one of the two antennas in the array. The radiation pattern of the second antenna is a mirror image of the first.

The most noticeable effect on the radiation pattern is that the gain in the azimuthal plane in Fig. 5.4(a) is not circular. For both the copper and conductive polymer arrays, the pattern is more oval shaped in the horizontal direction. This "squeezing" effect corresponds to the perturbation of the near field, or mutual coupling, by the proximity of the second antenna. The mutual coupling has a stronger effect with the copper antennas because the metal is more conductive than the polymer antennas. From the azimuthal plane in Fig. 5.4(a), the copper antenna has a maximum gain of 2.5 dBi, whereas the conductive polymer antenna has a maximum gain of -1.5 dBi. This lower gain is due to the lower conductivity of the polymer.

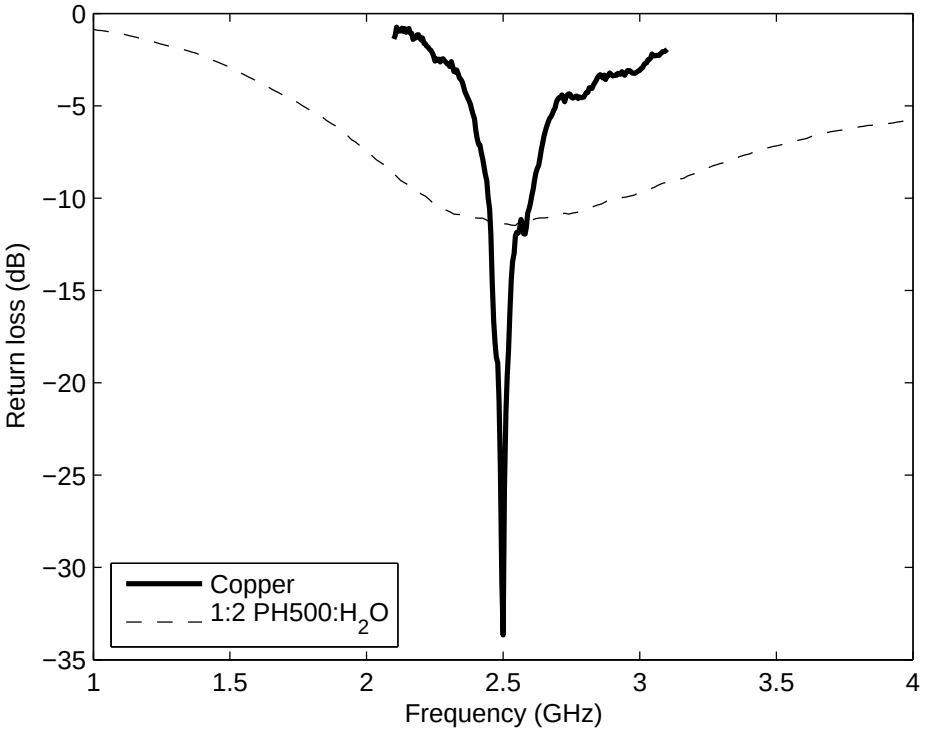

Figure 5.3: Measured return loss for a copper antenna and a transparent conductive polymer antenna

Greater analysis of the effect of transparency and antenna gain is provided in Sec. 5.5.

In the elevation plane, shown in Fig. 5.4(b), the conductive polymer antennas are roughly 4 dB lower than the copper antennas. There are nulls at the top and bottom of the antenna due to the electromagnetics of dipoles [56].

5.5 Flexibility and Transparency

Clearly, conductive polymer antennas have lower gain than copper antennas. However, conductive polymers are flexible and can be transparent, which makes them candidates for systems that require less conspicuous antenna systems. In this section, the flexibility and transparency of the conductive polymer antennas is analyzed.

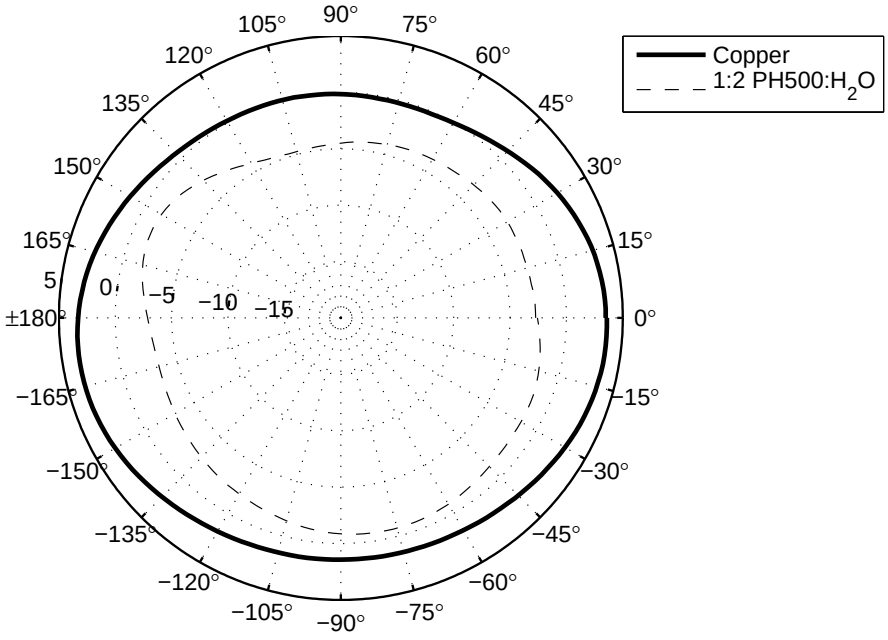

(a) Azimuthal angles and elevation angle of 90°

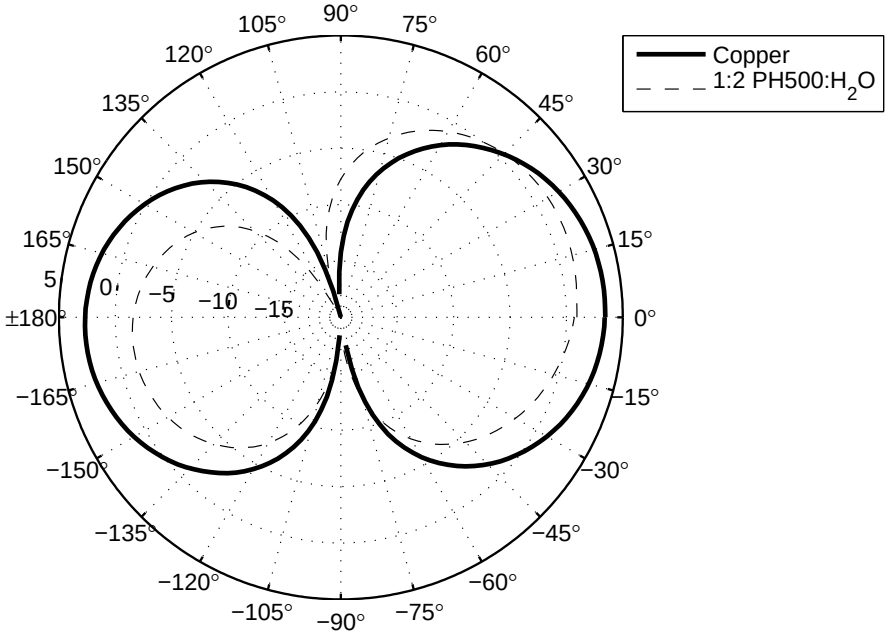

(b) Elevation angles and azimuthal angle of 0°

Figure 5.4: A comparison of the radiation patterns of a copper and a conductive polymer MIMO antenna arrays

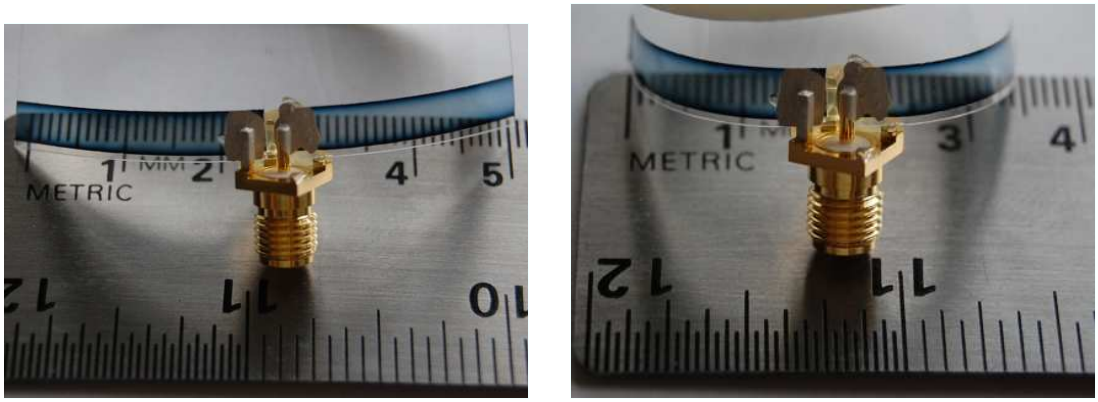

(a) Bend length: 50mm (b) Bend length: 35mm

Figure 5.5: Picture of a conductive polymer antenna with different amounts of bending

5.5.1 Flexibility

To consider how flexing a conductive polymer antenna affects the performance, the radiation pattern was measured for varying degrees of bend θ. The antenna substrate is bent and held in place, such that distance between the two edges of the substrate is less that the length of the substrate [57]. Based upon the geometry of a circle, the angle can be calculated from the length of the substrate (arc length) and the length of the chord. The amount of bend applied to the antennas is shown in Fig. 5.5. The antennas were tested with: no bend (substrate of length 60mm), a bend of chord length 50mm or $\theta = 160°$, and a bend of chord length 35mm or $\theta = 95°$.

The MIMO radiation patterns of the full strength conductive polymer antennas are shown in Fig. 5.6 for decreasing values of θ or increasing bend. When the antenna is not bent the angle is 180°. As the antenna becomes more bent, the angle decreases. From the azimuthal plane in Fig. 5.6(a), it is shown that an increase in bending has a minimal effect on the radiation pattern. Without any bending, the antenna has a maximum of 1 dBi. With bending, the maximum gain of the antenna is 1 dB lower. It is important to note that relative omni-directional shape is still present.

However, bending the antenna does have a greater affect on the elevation plane seen in Fig. 5.6(b). Bending the antenna distorts the pattern reducing the severity of the nulls and creating a more omni-directional pattern in the elevation plane. The bend changes the current distribution of the antenna, which creates an electrically short, or Hertzian dipole. The broadside gain is slightly lower because the gain is higher where would normally be nulls in the radiation pattern.

5.5.2 Transparency

Changing the functional thickness through dilution has an effect of the conductivity and transparency. There is a tradeoff between having high conductivity and high transparency. The different levels of dilution are: full strength PH500, 1:1 PH500:H_2O, and 1:2 PH500:H_2O. These dilutions are in order of decreasing conductivity. The tradeoff between conductivity and transparency can be seen by analyzing the return loss for the different solutions in Fig. 5.7. The full strength and 1:1 solutions are very good, while the 1:2 solution is just below -10 dB. However, the 1:2 is much more transparent as seen in Fig. 5.2 and analyzed later in this section.

To show how the characteristics of the antenna are effected by conductivity, radiation patterns were measured. In Fig. 5.8, the radiation patterns for three different levels of conductive polymer antenna arrays are shown in comparison with a copper array. In the azimuthal plane in Fig. 5.8(a), the copper array has a maximum gain of 3 dB higher than the full strength solution. The 1:1 solution is similar to the full strength polymer with a gain of 0.5 dBi. The weakest solution and most transparent, 1:2, has a gain of -1.5 dBi. The elevation plane is shown Fig. 5.8(b) and has the same result, which is that the most transparent antenna has the lowest gain, or conductivity.

To analytical show the transparency of the different antennas, the antennas were

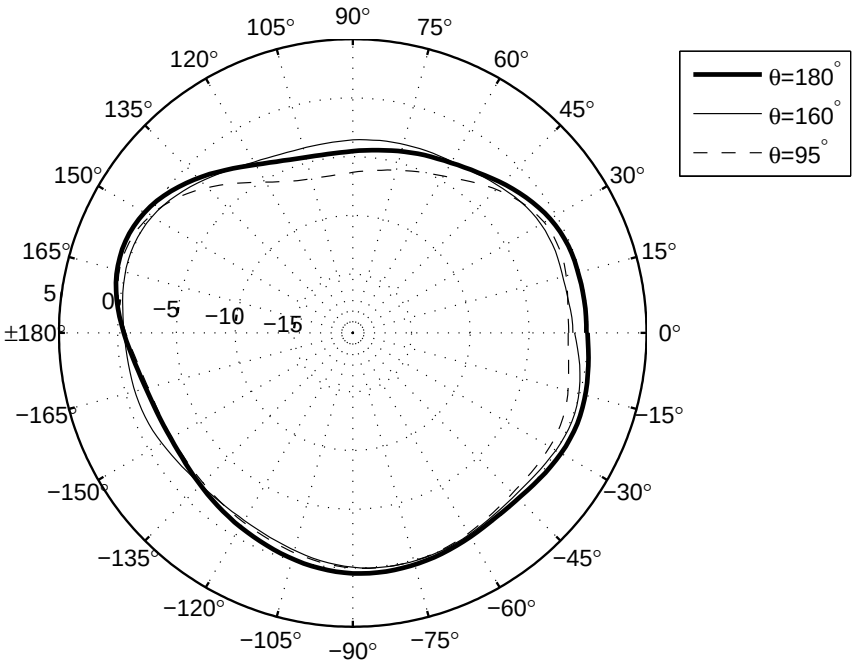

(a) Azimuthal angles and elevation angle of 90°

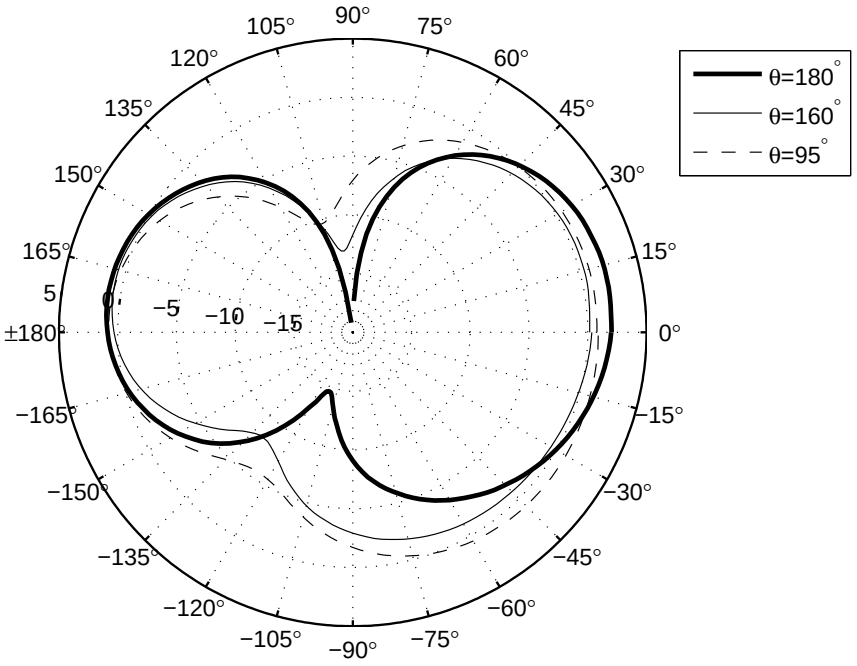

(b) Elevation angles and azimuthal angle of 0°

Figure 5.6: A comparison of the radiation patterns of a MIMO conductive polymer antenna array with a decreasing bend in the substrate: $\theta = 180°$, $\theta = 160°$, $\theta = 95°$.

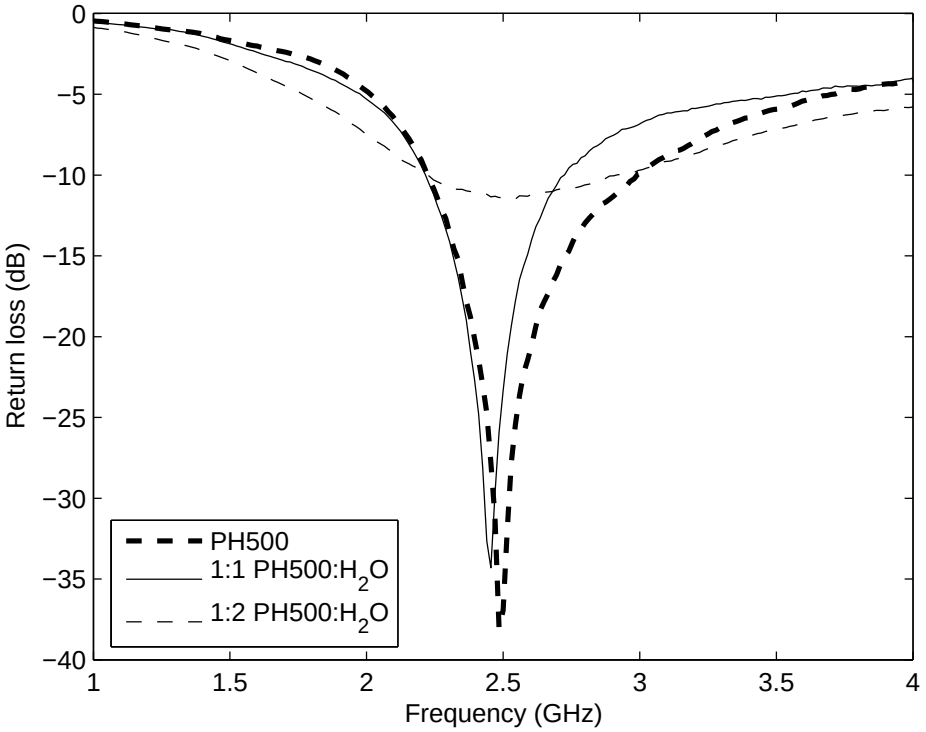

Figure 5.7: Measured return loss of the conductive polymer antennas with different levels of dilution

measured with an Ocean Optics USB2000 spectrometer. The percent of visible spectrum is shown in Fig. 5.9. The wavelengths of 400 and 800 nm correspond to the colors blue and red respectively. The full strength PH500 has at best 5% transparency (highest gain). The 1:1 dilution is much higher at a maximum of 30%. With a dilution ratio of 1:2 polymer to water, between 40 and 80 precent of visible light passes through the antenna at different optical wavelengths.

5.6 Network Performance

The characteristics of conductive polymer antenna arrays have been shown to be similar to copper arrays, though with lower gain. However, it is interesting to understand the performance of the conductive polymer antennas in a realistic situation. To analyze the performance of conductive polymer MIMO antennas channel sounding

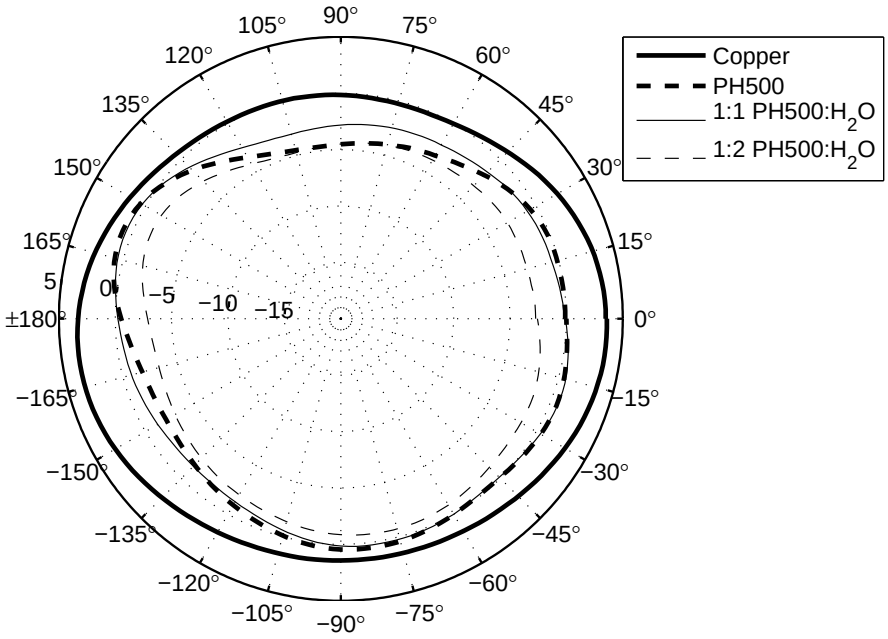

(a) Azimuthal angles and elevation angle of 90°

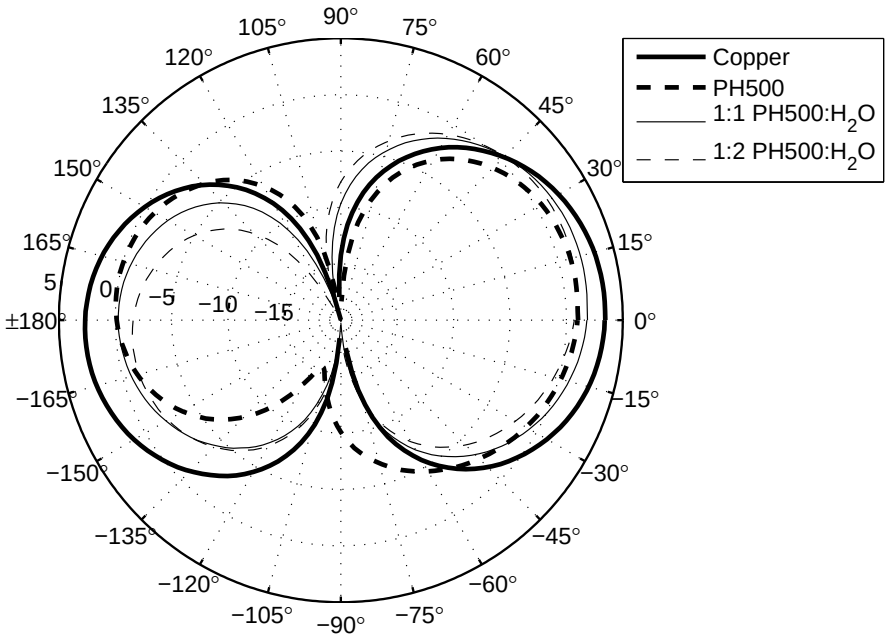

(b) Elevation angles and azimuthal angle of 0°

Figure 5.8: A comparison of the radiation patterns of MIMO polymer antenna arrays with a decreasing conductivity: Copper, full strength PH500, 1:1 PH500:H_2O, and 1:2 PH500:H_2O.

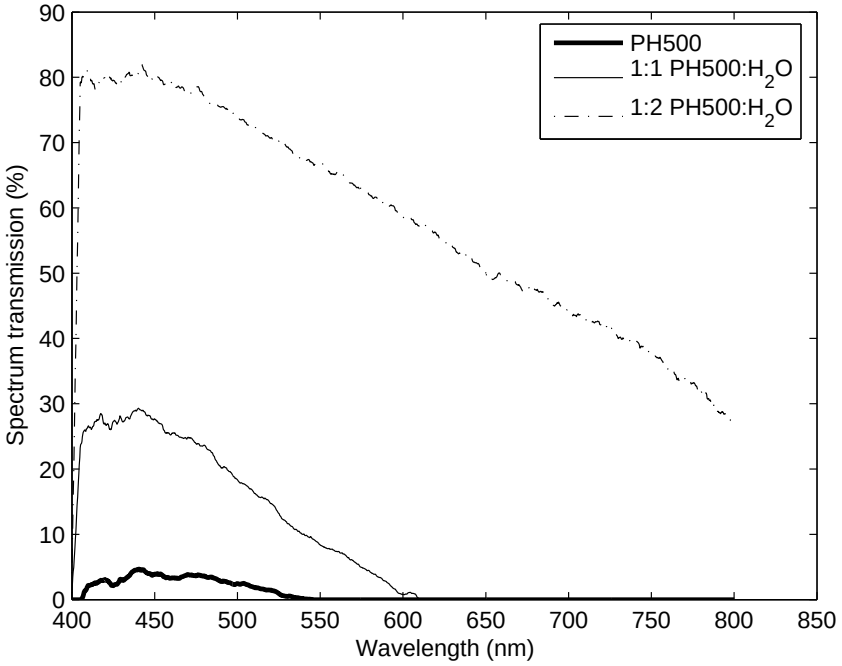

Figure 5.9: Percent of optical transmission through the dipole conductive polymer antenna for: full strength PH500, 1:1 PH500:H_2O, and 1:2 PH500:H_2O

measurements were performed to investigate the maximum capacity achievable with the conductive polymer antennas. Also, packet error rate test we done to understand the actual performance of the antennas in a link.

5.6.1 MIMO Network Capacity

For the channel sounding experiment, three different scenarios were measured to compare the results of the 1:2 dilution conductive polymer MIMO antenna array in a line-of-sight (LOS) and non-line-of-sight (NLOS) configuration as seen in Fig. 5.10. For each of the three scenarios, there were three co-channel interference limited links. In the diagram of the 3^{rd} floor of the Bossone building, each link has its own color, the transmitters are squares, the receivers are circles, and the line through each node represents the orientation of the linear uniform MIMO array. NLOS links are shown as dashed lines and LOS are solid lines. The interfering links are not included

to simplify the visualization; however all links between all transmitter and receiver pairs were measured. The spacing was chosen to be $\lambda/4$ to match the dimension of mobile devices used for 802.11n and 802.16e. After performing the channel sounding measurement, the capacity is calculated with (2.6), which includes interference. For simplicity, only equal power allocation was used.

The average link capacity for the first scenario (with two NLOS links) is shown in Fig. 5.11. In this scenario, the capacity over SNR is similar for each of the degrees of bend. The greatest amount of bend is however, higher than the degrees of bend. Because there is two NLOS links, there will be more energy scattered through the environment. Therefore, with the close antenna spacing greater perturbation in the radiation pattern will lead to higher capacity. As previously shown, the largest bend has the most variation in the radiation pattern.

The capacity for the second scenario was chosen to have one NLOS link with a transmitter close to one of the receivers. The third scenario was chosen to have only LOS links, with receivers far from the interfering transmitters. The average per link capacity for these two scenarios is shown in Fig. 5.12 and Fig. 5.13. Both of these scenarios have similar capacities and the unbent antenna arrays have the highest capacity. The capacity is higher because the gain of these antennas is higher, which is more important in LOS conditions.

5.6.2 Packet Error Rate

Finally, the conductive polymer antennas were used in real-time MIMO communications system to evaluate the antenna performance by measuring the packet error rate. The packet error rate is determined by transmitting a large number of packets and counting the number in errors over varying transmit power. The signal-to-noise ratio was calculated by analyzing the the power spectral density of a series of transmitted

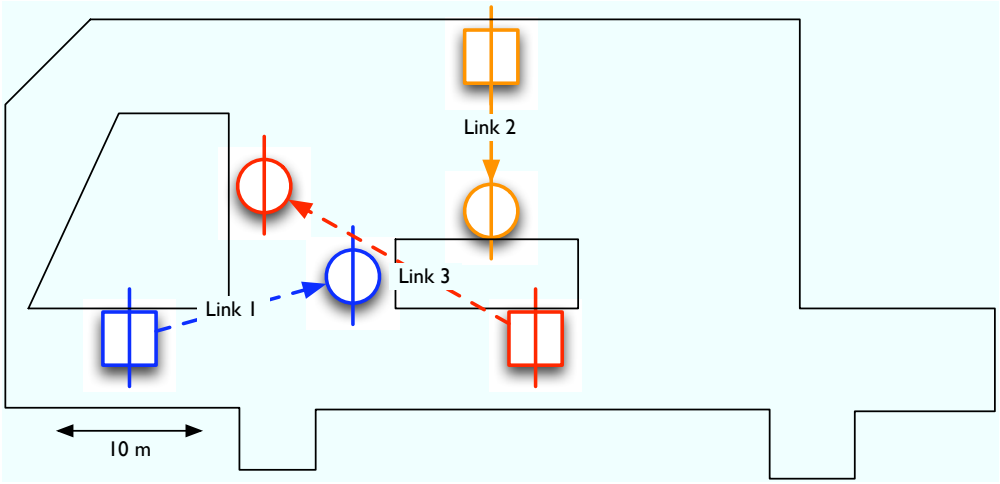

(a) Topology 1

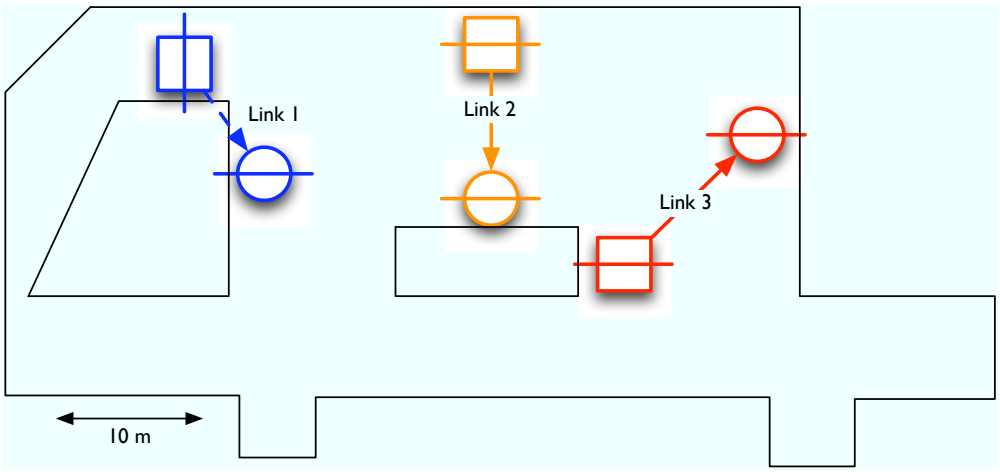

(b) Topology 2

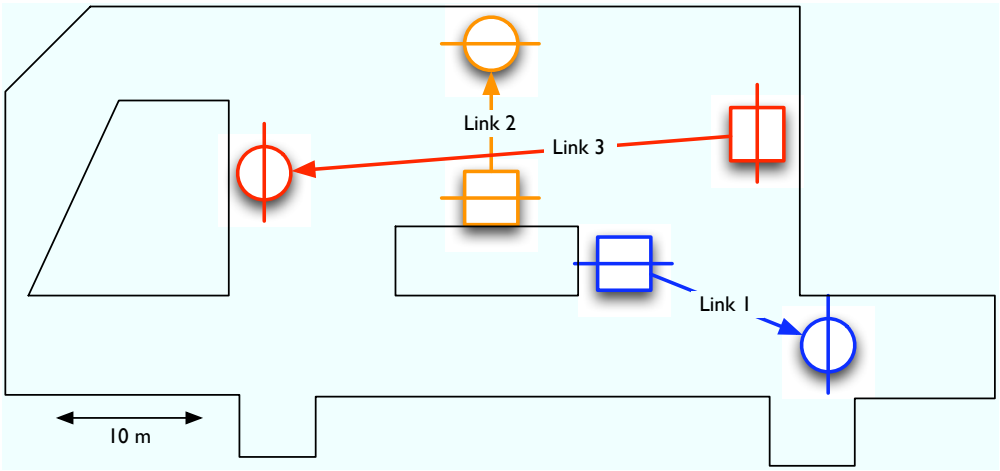

(c) Topology 3

Figure 5.10: Scenarios used for measurements the MIMO network performance of a conductive polymer antenna array

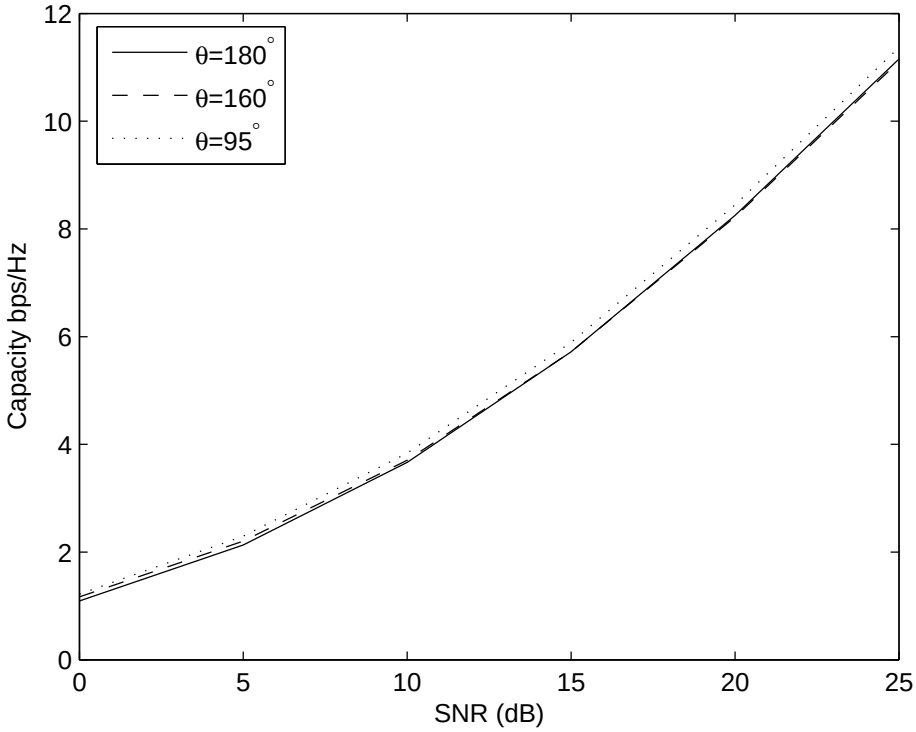

Figure 5.11: Link capacity of scenario #1 using MIMO transparent antennas

1's and 0's. The modulation scheme used was QAM, a packet length of 1024, and coding rate 1/2. The PER measured for the conductive polymer antennas and copper array both had 0 packets dropped when the SNR was greater than 8 dB.

5.7 Conclusion

In this chapter, antennas fabricated with conductive polymers for a MIMO communication system were presented. Conductive polymers can be printed cheaply and easily in a manner such that they are transparent and flexible. The co-planar antenna design simplifies the fabrication process because it is single sided. This also aides in creating transparent antennas. While the conductive polymer antennas do not radiate as well as copper antennas, they do offer flexibility and transparency. The performance of the antennas with various amounts of bending and conductivity were

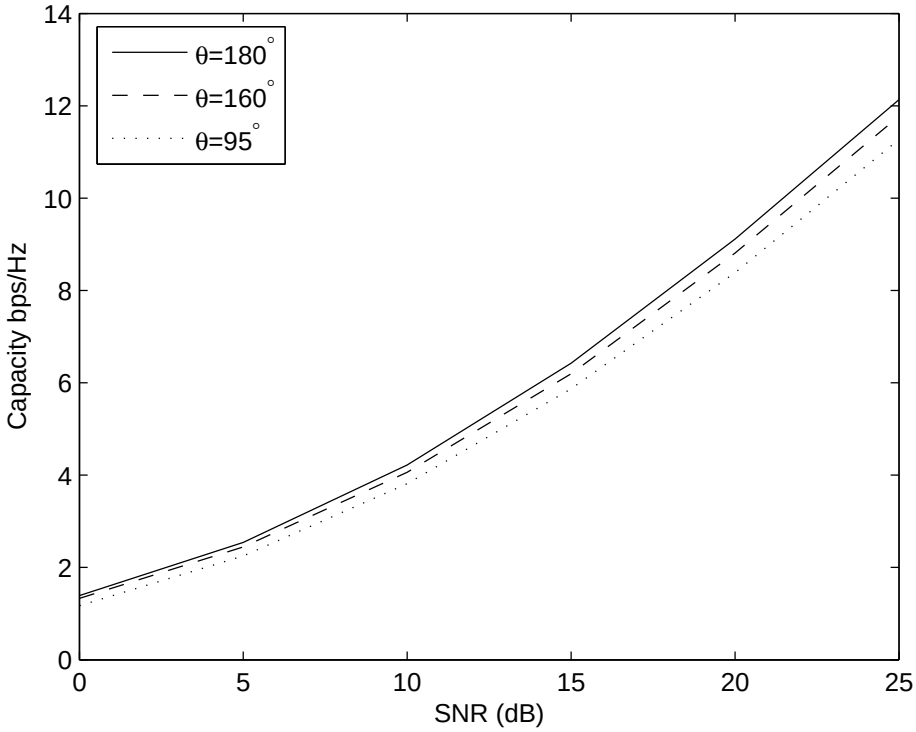

Figure 5.12: Link capacity of scenario #2 using MIMO transparent antennas

compared. Channel sounding measurements were made to evaluate the antennas in a practical system. These results show that conductive polymer antenna arrays can be used when unobtrusive antenna systems are required.

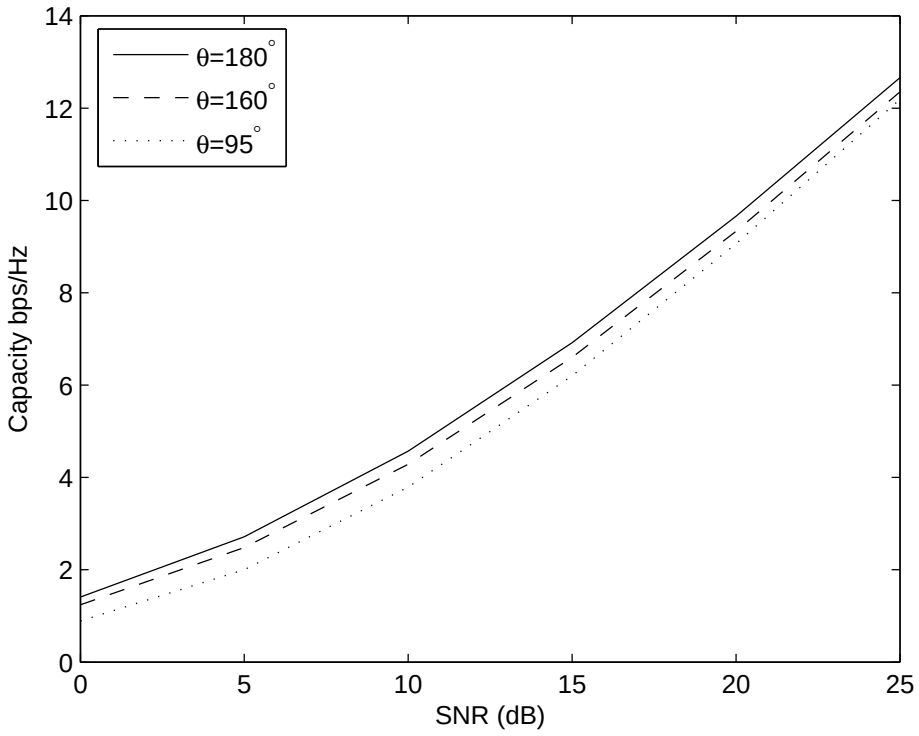

Figure 5.13: Link capacity of scenario #3 using MIMO transparent antennas

Chapter 6. Conclusion

Multiple-input multiple-out (MIMO) communication systems are capable of increasing capacity in wireless networks by adding multiple transceivers to each. In practice, there are limitations that affect the capacity. These limitations include the co-channel interference, the spacing of the antennas, and integration of the multiple transceivers in a node. This dissertation presents several methods with the use of power allocation and antenna spacing for increasing the performance of MIMO communication systems limited by co-channel interference. Further, the optically transparent, flexible antenna arrays were designed as an enabling technology to make the required spacing of the antenna arrays less obtrusive. The methods presented were simulated and validated with a software-defined radio multiple antenna testbed.

For networks limited by co-channel interference, several power allocation methods to increase the capacity were presented. These distributed and centralized methods require different amounts of channel information. The contribution of the dissertation is the experimental performance of different power allocation methods. These experiments show that the game theoretic (GT) method has higher capacity than the other distributed methods, but lower capacity than the centralized gradient projection (GP) method. The efficiency of the GT method approaches the efficiency of the GP method. These results aide in understanding how power allocation can be effectively used to increase capacity in MIMO ad hoc networks.

Another important aspect of MIMO systems is the physical properties of antenna array. The antenna array directly affects the wireless channel, thus the capacity. Previous work for single link communications showed that wide spacing is preferable because it decorrelates the channel, which increases the capacity. However, in co-channel interference limited networks, greater spacing may not always be better

because the interference also becomes more decorrelated. The contribution of this dissertation is to show a method for decomposing the wireless channel to understand how the spacing of the antennas and the number of interferers effects communications. By understanding these effects, we have shown the capacity can be increased depending on the network conditions. The analysis of the wireless channel and the capacity results were simulated and measured for an indoor ad hoc network.

For next generation mobile communication systems that use multiple antennas, incorporation of the antenna array into the device becomes a challenge due the physical size of the antennas and the array. We present a multiple antenna array with antennas fabricated with conductive polymer. Conductive polymer antennas are flexible and can be printed such that they are optically transparent. These features make integration of multiple antennas into a mobile system easier. The performance of conductive polymer antenna arrays is characterized in comparison to a conventional copper array. The characteristics of the antennas with different degrees of bend and transparency are also shown. Channel measurements show that bending the antennas have a limited effect on the capacity in an ad hoc network. While conductive polymer antennas have lower gain when compared to copper antennas, conductive polymer antennas are less obtrusive and can be more easily incorporated into mobile systems.

In short, this dissertation presents experimental results for increasing the quality of multiple antenna communication systems. By controlling the power, antennas array dimensions, and form factor, we can reach the growing demand for faster and more ubiquitous communications.

Bibliography

[1] C. E. Shannon, "Communication in the presence of noise," *Proceedings of the IRE*, vol. 37, no. 1, pp. 10–21, Jan. 1949.

[2] ——, "A mathematical theory of communication," *SIGMOBILE Mob. Comput. Commun. Rev.*, vol. 5, no. 1, pp. 3–55, 2001.

[3] J. E. Katz and M. A. Aakhus, *Perpetual contact: mobile communication, private talk, public performance*. Cambridge University Press, 2002.

[4] N. J. Kirsch, C. Liang, and K. R. Dandekar, "Experimental characterization of resource allocation algorithms in MIMO-OFDM ad hoc networks," in *Proceedings of the IEEE Radio and Wireless Symposium*, 2007.

[5] N. J. Kirsch, J. Kountouriotis, C. Liang, and K. R. Dandekar, "Experimental evaluation of game theoretic power allocation in MIMO ad-hoc networks," *Wireless Communications, IEEE Transactions on*, vol. 8, no. 5, pp. 2292–2295, May 2009.

[6] N. J. Kirsch, J. Kountouriotis, and K. R. Dandekar, "Analysis of antenna spacing in MIMO channels with co-channel interference," *in preparation for IEEE Transactions on Vehicular Technology*, 2009.

[7] N. J. Kirsch, N. A. Vacirca, E. E. Plowman, T. P. Kurzweg, A. K. Fontecchio, and K. R. Dandekar, "Optically transparent conductive polymer RFID meandering dipole antenna," in *RFID, 2009 IEEE International Conference on*, April 2009, pp. 278–282.

[8] N. J. Kirsch, N. A. Vacirca, E. E. Plowman, K. R. Dandekar, A. K. Fontecchio, and T. P. Kurzweg, "Translucent conformal conductive polymer dipole antenna," *in preparation for IEEE Transactions on Antennas and Propagation*, 2009.

[9] G. J. Foschini and M. J. Gans, "On the limits of wireless communications in a fading environment when using multiple antennas," *Wireless Personal Communications*, vol. 6, pp. 331–335, Mar. 1998.

[10] M. A. Jensen and J. W. Wallace, "A review of antennas and propagation for MIMO wireless communications," *IEEE Transactions on Antennas and Propagation*, vol. 52, no. 11, pp. 2810 – 24, Nov. 2004.

[11] S. Vishwanath, N. Jindal, and A. Goldsmith, "Duality, achievable rates, and sum-rate capacity of gaussian MIMO broadcast channels," *Information Theory, IEEE Transactions on*, vol. 49, no. 10, pp. 2658–2668, Oct. 2003.

[12] A. Molisch, M. Win, Y.-S. Choi, and J. Winters, "Capacity of MIMO systems with antenna selection," *Wireless Communications, IEEE Transactions on*, vol. 4, no. 4, pp. 1759–1772, July 2005.

[13] T. M. Cover and J. A. Thomas, *Elements of information theory*. New York, NY: Wiley, 1991.

[14] S. Ye and R. S. Blum, "Optimized signaling for MIMO interference systems with feedback," *IEEE Transactions on Signal Processing*, vol. 51, pp. 2839–2848, Nov. 2003.

[15] R. Blum, "MIMO capacity with interference," *IEEE J. Selected Areas Commun.*, vol. 21, pp. 793–801, June 2003.

[16] C. Liang and K. R. Dandekar, "Power management in MIMO ad hoc networks: a game-theoretic approach," *IEEE Transactions of Wireless Communications*, vol. 6, no. 4, pp. 2839–2848, Apr. 2007.

[17] M. Webb, M. Beach, and A. Nix, "Capacity limits of MIMO channels with co-channel interference," in *2004 IEEE 59th Vehicular Technology Conference. VTC 2004-Spring*, vol. 2, 2004, pp. 703 – 7.

[18] C. Mias, C. Tsakonas, N. Prountzos, D. Koutsogeorgis, S. Liew, C. Oswald, R. Ranson, W. Cranton, and C. Thomas, "Optically transparent microstrip antennas," in *Antennas for Automotives, IEE Colloquium on*, 2000, pp. 8/1–8/6.

[19] R. Van Nee and R. Prasad, *OFDM for wireless multimedia communications*. Artech House, 2000.

[20] The Click Modular Router Project. [Online]. Available: http://pdos.csail.mit.edu/click/

[21] F. S. de Adana, O. Gutierrez, I. G. Diego, J. P. Arriaga, and M. Catedra, "Propagation model based on ray tracing for the design of personal communication systems in indoor environments," *IEEE Trans. on Vehicular Technology*, vol. 49, no. 6, pp. 2105–2112, Nov. 2000.

[22] M. Catedra and J. Perez-Arriaga, *Cell Planning for Wireless Communications*. Boston, Massachusetts: Artech House, 1999.

[23] D. Davidson, I. Theron, U. Jakobus, F. Landstorfer, F. Meyer, J. Mostert, and J. V. Tonder, "Recent progress on the antenna simulation program FEKO," in *1998 South African Symposium on Communications and Signal Processing*, vol. 1, Sept. 1998, pp. 427–430.

[24] W. Yu, W. Rhee, S. Boyd, and J. Cioffi, "Iterative water-filling for gaussian vector multiple access channels," *IEEE Trans. Infor. Theory*, vol. 50, pp. 145–152, Jan. 2004.

[25] M. Demirkol and M. Ingram, "Power-controlled capacity for interfering MIMO links," in *Proceedings of Vehicular Techonology Conference*, vol. 1, Sept. 2001, pp. 187–191.

[26] G. Scutari, D. Palomar, and S. Barbarossa, "Competitive design of multiuser MIMO systems based on game theory: a unified view," *Selected Areas in Communications, IEEE Journal on*, vol. 26, no. 7, pp. 1089–1103, September 2008.

[27] M. Ozdemir, E. Arvas, and H. Arslan, "Dynamics of spatial correlation and implications on MIMO systems," *Communications Magazine, IEEE*, vol. 42, no. 6, pp. S14–S19, June 2004.

[28] "Mobile Networked MIMO (MNM) Web Site." [Online]. Available: http://www.darpa.mil/ato/solicit/MNM/overview.htm

[29] K. Dandekar and R. H. Jr., "Large-scale capacity characterization of smart antenna equipped mobile ad-hoc network nodes in an urban network," in *Proc. of IEEE Military Communications Conference*, 2003.

[30] D. Popescu and C. Rose, *Interference Avoidance Methods for Wireless Systems*. New York, NY: Kluwer Academic/Plenum Publishers, 2004.

[31] J.-S. Jiang, M. F. Demirkol, and M. A. Ingram, "Measured capacities at 5.8 GHz of indoor MIMO systems with MIMO interference," *IEEE Vehicular Technology Conference*, vol. 58, no. 1, pp. 388 – 393, 2004.

[32] M. F. Demirkol, M. A. Ingram, and Z. Yun, "Feasibility of closed loop operation for MIMO links with MIMO interference," *IEEE Antennas and Propagation Society, AP-S International Symposium (Digest)*, vol. 4, pp. 3669 – 3672, 2004.

[33] A. M. Tulino, A. Lozano, and S. Verdu, "Impact of antenna correlation on the capacity of multiantenna channels," *IEEE Transactions on Information Theory*, vol. 51, no. 7, pp. 2491 – 509, July 2005.

[34] A. Forenza, D. J. Love, and R. H. Jr., "Simplified spatial correlation models for clustered MIMO channels with different array configurations," *IEEE Transactions on Vehicular Technology*, vol. 56, no. 4, pp. 1924 – 34, July 2007.

[35] T. Svantesson, "Correlation and channel capacity of MIMO systems employing multimode antennas," *IEEE Transactions on Vehicular Technology*, vol. 51, no. 6, pp. 1304 – 12, Nov. 2002.

[36] R. H. Y. Louie, M. R. McKay, I. B. Collings, and B. Vucetic, "Capacity approximations for multiuser MIMO-MRC with antenna correlation," in *IEEE International Conference on Communications 2007*, June 2007, pp. 5195–5200.

[37] D. Chizhik, F. Rashid-Farrokhi, J. Ling, and A. Lozano, "Effect of antenna separation on the capacity of BLAST in correlated channels," *Communications Letters, IEEE*, vol. 4, no. 11, pp. 337–339, Nov 2000.

[38] D. Browne, M. Manteghi, M. Fitz, and Y. Rahmat-Samii, "Experiments with compact antenna arrays for mimo radio communications," *IEEE Transactions on Antennas and Propagation*, vol. 54, no. 11, pp. 3239 – 50, Nov. 2006.

[39] A. Goldsmith, S. Jafar, N. Jindal, and S. Vishwanath, "Capacity limits of MIMO channels," *Selected Areas in Communications, IEEE Journal on*, vol. 21, no. 5, pp. 684–702, June 2003.

[40] P. Smith, S. Roy, and M. Shafi, "Capacity of MIMO systems with semicorrelated flat fading," *Information Theory, IEEE Transactions on*, vol. 49, no. 10, pp. 2781–2788, Oct. 2003.

[41] W. Weichselberger, M. Herdin, H. Ozcelik, and E. Bonek, "A stochastic MIMO channel model with joint correlation of both link ends," *Wireless Communications, IEEE Transactions on*, vol. 5, no. 1, pp. 90–100, Jan. 2006.

[42] J. S. Kwak, J. G. Andrews, and A. Lozano, "MIMO capacity in correlated interference-limited channels," in *Information Theory, IEEE International Symposium on*, June 2007, pp. 106–110.

[43] J. Liu, Y. Hou, Y. Shi, H. Sherali, and S. Kompella, "On the capacity of multiuser MIMO networks with interference," *Wireless Communications, IEEE Transactions on*, vol. 7, no. 2, pp. 488–494, February 2008.

[44] A. Moustakas, S. Simon, and A. Sengupta, "MIMO capacity through correlated channels in the presence of correlated interferers and noise: a (not so) large n analysis," *Information Theory, IEEE Transactions on*, vol. 49, no. 10, pp. 2545–2561, Oct. 2003.

[45] R. A. Horn and C. R. Johnson, *Topics in matrix analysis.* New York, NY: Cambridge University Press, 2007.

[46] D. Gesbert, M. Kountouris, R. Heath, C.-B. Chae, and T. Salzer, "Shifting the MIMO paradigm," *Signal Processing Magazine, IEEE*, vol. 24, no. 5, pp. 36–46, Sept. 2007.

[47] P. Almers, E. Bonek, N. Czink, M. Debbah, V. Degli-Esposti, H. Hofstetter, P. Kysti, D. Laurenson, G. Matz, A. F. Molisch, C. Oestges, and H. zcelik, "Survey of channel and radio propagation models for wireless MIMO systems," *EURASIP Journal on Wireless Communications and Networking*, 2007.

[48] A. Ghosh, D. Wolter, J. Andrews, and R. Chen, "Broadband wireless access with wimax/802.16: current performance benchmarks and future potential," *Communications Magazine, IEEE*, vol. 43, no. 2, pp. 129–136, Feb. 2005.

[49] F. Lalezari, "Conformal antenna and method," U.S. Patent 4 816 836, March, 1989. [Online]. Available: http://www.freepatentsonline.com/4816836.html

[50] S. Cichos, J. Haberland, and H. Reichl, "Performance analysis of polymer based antenna-coils for RFID," in *IEEE Conference on Polymers and Adhesives in Microelectronics and Photonics*, 2002, pp. 120 – 4.

[51] H. Rmili, J.-L. Miane, H. Zangar, and T. Olinga, "Design of microstrip-fed proximity-coupled conducting-polymer patch antenna," *Microwave and Optical Technology Letters*, vol. 48, no. 4, pp. 655 – 660, 2006.

[52] P. Nikitin, S. Lam, and K. Rao, "Low cost silver ink RFID tag antennas," in *IEEE Antennas and Propagation Society International Symposium*, vol. 2B, 2005, pp. 353 – 6.

[53] N. Outaleb, J. Pinel, M. Drissi, and O. Bonnaud, "Microwave planar antenna with RF-sputtered indium tin oxide films," *Microwave and Optical Technology Letters*, vol. 24, no. 1, pp. 3–7, 2000.

[54] (2008) Clevios PDOT-PSS. [Online]. Available: http://www.clevios.com/index.php?page_id=955

[55] (2008) PChem nano ink. [Online]. Available: http://www.nanopchem.com/Products.html

[56] C. A. Balanis, *Antenna Theory: Analysis and Design*. Wiley, 1997.

[57] S. Raffaelli, Z. Sipus, and P.-S. Kildal, "Analysis and measurements of conformal patch array antennas on multilayer circular cylinder," *Antennas and Propagation, IEEE Transactions on*, vol. 53, no. 3, pp. 1105–1113, March 2005.

Appendix A. Table of Symbols

Symbol	Definition
N_r	Number of receive antennas
N_t	Number of transmit antennas
$\mathcal{L}$	Set of all links
L	Number of links in the network
l	Link of interest
$\mathbf{y}_l$	Receive signal vector with size $N_r \times 1$
$\mathbf{x}_l$	Transmit signal vector with size $N_t \times 1$
$\mathbf{H}_{l,j}$	Channel matrix with size $N_r \times N_t$
$\mathbf{n}_l$	Gaussian noise vector with size $N_r \times 1$
d	Distance between antenna elements
a_l	Normalization factor
K	Number of OFDM subcarriers
C_l	Capacity of link l (bps/Hz)
C	Sum-rate capacity (bps/Hz)
$\mathbf{R}_l$	Interference-plus-noise covariance matrix with size $N_r \times N_t$
ϵ_r	Relative permittivity
μ_r	Relative permeability
λ	Wavelength
$\mathbf{Q}_l$	Power allocation matrix
P	Total power available
$\mathbf{U}$	Unitary "input" matrix from the singular value decomposition
$\mathbf{V}$	Unitary "output" matrix from eigenvalue decomposition
$\mathbf{V}_w$	Whitened unitary matrix from eigenvalue decomposition
$\mathbf{\Lambda}$	Diagonal matrix of the eigenvalues
μ	Water level
$\mathbf{H}_w$	Whitened channel
u_l	Utility function
γ_l	Pricing factor
P_l	Power constraint per link
σ	Squared singular value
$p_{i,l}$	Power level per link l and transmitter i
$f(x)$	Function of x
s_i^j	i^{th} singular value of $\mathbf{\Lambda}$ of the j^{th} channel
R^i	Ratio of the singular values of channel i
S^i	Sum of the squared singular values of channel i
n_i	i^{th} singular value of $\mathbf{R}_l$

Appendix B. Table of Acronyms

Acronym	Definition
BER	Bit error rate
BPSK	Binary shift-keying
CCI	Co-channel interference
CDF	Cumulative distribution function
DI	Deionized water
DMSO	Dimethyl sulfoxide
GT	Game theoretic method
GGP	Global gradient projection method
LOS	Line of sight
INR	Interference-to-noise ratio
ITO	Indium tin oxide
IWF	Independent waterfilling
MAC	Medium access layer
MIMO	Multiple-input multiple-output
MUWF	Multi-user waterfilling
NLOS	Non-line of sight
OFDM	Orthogonal frequency division multiplexing
PET	Polyethylene terephthalate
PHY	Physical layer
RF	Radio frequency
SIR	Signal-to-interference ratio
SNR	Signal-to-noise ratio
SDM	Spaced division multiplexing
SDR	Software defined radio
WLAN	Wireless local area network

Vita

Nicholas J. Kirsch was born in Wauwatosa, Wisconsin, USA on May 17, 1980. He obtained his B.S. degree in Electrical Engineering from the University of Wisconsin - Madison in May 2003. Nicholas subsequently joined the Department of Electrical and Computer Engineering at Drexel University in Philadelphia, Pennsylvania and has been affiliated with the Wireless Systems Laboratory ever since. In June of 2006, he received an M.S. degree in Electrical Engineering and Telecommunications from Drexel University. His research interests include MIMO communications, ad hoc networking, adaptive radio systems, and RFID antenna design.

In 2001 and 2002, Nicholas worked for W.L. Gore & Associates on fiber optic link modules and long-wavelength lasers. He was a teaching assistant for several undergraduate courses and was an instructor for one undergraduate and two graduate courses. Nicholas also worked with Applied Communication and Information Networking group in Camden, NJ.

His research has lead to the publication of three journal papers and three conference papers. In 2006, he was awarded the Koerner Family Fellowship at Drexel University. In 2007, Nicholas was a student paper finalist for his paper at the Radio and Wireless Symposium and he was awarded the Excellence in Research Award at Drexel University. He is a reviewer for IEEE Transactions on Vehicular Technology and the Communication Theory Symposium. Nicholas is a member of IEEE and AAAS.